

T₁ MAPPING FOR DCE-MRI

A dissertation submitted to the Faculty of Medicine, University of Malaya in partial fulfillment of the requirements for the degree of Master of Medical Physics

By

NURUN NAJWA BINTI KAMALUZAMAN

Department of Biomedical Imaging

Faculty of Medicine

University of Malaya

Kuala Lumpur

Malaysia

2013

DISCLAIMER

I declare that this project report records the results of investigations performed by me, that it is of my own composition, that is has not been submitted previously for a higher degree in any university.

.....

Nurun Najwa binti Kamaluzaman

May 2013

ABSTRACT

The main purpose of this study is to develop a T_1 mapping technique by using variable flip angle (VFA) technique based on fast spoiled gradient echo (FSPGR) pulse sequence and to implement the technique in *in vivo* imaging. FSPGR imaging was performed on a set of T_1 gel phantoms with different concentrations of Gd_3Cl by using 1.5 Tesla MRI. To determine the T_1 values of the gel phantoms, signal intensities from three sets of images produced by using three different flip angles were fitted pixel-by-pixel by using spoiled gradient echo equation. The T_1 values calculated were displayed as a T_1 map. The T_1 values of the gel phantoms estimated with selected ROI were compared with the values determined by a standard T_1 measurement technique i.e. inversion recovery [TR = 6500 ms, TE = 7.51 ms, inversion time (TI) = 50, 300, 550, 800, 1050 ms]. The VFA mapping was then performed on four healthy volunteers to assess its effectiveness in clinical imaging. The mapping was performed on the right thigh of the volunteer for two different anatomical orientations, axial and coronal. The T_1 values of the fat and muscle estimated with selected ROI were compared with different orientations, scanning dimensions and pulse sequences. The comparison of T_1 value for different orientation was performed for three pulse sequences i.e., Multislice Two Dimensional (M2D) FSPGR, three

dimensional (3D) FSPGR and Liver acceleration volume acquisition (3D LAVA) at axial and coronal orientations. The comparison of T_1 value for scanning technique was performed using M2D FSPGR and 3D FSPGR pulse sequences. The comparison of T_1 value for different pulse sequence was performed using 3D FSPGR and 3D LAVA pulse sequences. The curve fitting and image analysis were performed by using Matlab software. The T_1 values of the gel phantoms produced by using VFA technique of 3D FSPGR and 3D LAVA were close to the values determined by the IR method. The T_1 values estimated by 2D FSPGR showed different values respect to IR method. The T_1 values produced on volunteer at axial orientation was higher than values at coronal orientation. The T_1 values estimated using 3D FSPGR and 2D FSPGR showed in large difference. The T_1 values estimated using 3D FSPGR and 3D LAVA pulse sequence showed a smaller difference. We have developed a technique to map the T_1 values by using VFA spoiled gradient echo technique. The technique has been successfully implemented on T_1 gel phantoms and healthy volunteers. Further works will include more volunteers for improve the validity of this study.

ACKNOWLEDGEMENT

In the name of Allah, the Most Gracious and the Most Merciful

Alhamdulillah, all praises to Allah for the strengths and His blessing in completing this dissertation. Special appreciation goes to my supervisor; Dr. Azlan Che Ahmad, for his supervision and constant support during two semester session 2012/2013. His invaluable help of constructive comments and suggestions throughout the experimental and thesis works have contributed to the success of this project.

I would like to express my sincere gratitude to the lecturers and staffs of Medical Physics, Faculty of Medicine, University of Malaya for their co-operation in given valuable information, supporting, suggestions and guidance in the compilation and preparation this dissertation.

Great deals appreciated go to my clinical co-supervisor Professor Dr. Basri Johan Jeet Abdullah, Professor Ng Kwan Hoong and Mr. Shahrin Nizam Daman Huri for reviewing my work throughout the process of conducting this dissertation. I also appreciate the team of MRI's radiographers, Madam Siti Salwa Azhar and Mr. Azwan Abdullah in helping out the period of data collection.

Finally, an honorable mention goes to my beloved family and friends for their endless love, prayers and encouragement. To those who indirectly contributed in this dissertation, your kindness means a lot to me. Thank you very much.

TABLE OF CONTENTS

	Page
APPROVAL AND DECLARATION SHEET	ii
ABSTRACT	iii
ACKNOWLEDGMENT	v
TABLE OF CONTENTS	vi
LIST OF FIGURES	ix
LIST OF TABLES	xii
LIST OF EQUATION	xiii
LIST OF APPENDICES	xiv
LIST OF SYMBOLS, ABBREVIATIONS OR NOMENCLATURE	xv

CHAPTER 1 INTRODUCTION

1.1	Background	1
1.2	Objectives	2
1.3	Literature Review	3
1.4	Theory	4
1.4.1	Spin-lattice relaxation (T_1)	4
1.4.2	DCE-MRI	6
1.4.3	Magnetic Resonance Imaging (MRI) pulse sequence	7
1.4.3.1	Spin Echo Pulse Sequence	7
1.4.3.1.1	Fast Spin Echo Inversion Recovery (FSE-IR)	9
1.4.3.2	Gradient Echo Pulse Sequence	10
1.4.3.2.1	Fast Spoiled Gradient echo (FSPGR)	12
1.4.3.2.2	Liver Acceleration of Volume Acquisition (LAVA)	12
1.4.4	2D versus 3D Image Acquisition	12

CHAPTER 2 METHODOLOGY

2.1	Imaging Experiment on Gel Phantoms	16
2.1.1	Image Analysis of Experiments on Gel Phantoms	18
2.2	Imaging Experiment on Volunteers	21
2.2.1	Volunteer Image analysis	23

CHAPTER 3 RESULT

3.1	Imaging Experiment on Gel Phantoms	24
3.1.1	Fast Spin Echo Inversion Recovery (FSE-IR)	24
3.1.2	Multislices 2D FSPGR (M2D FSPGR)	26
3.1.3	Three Dimensional Fast Spoiled Gradient Echo (3D FSPGR)	27
3.1.4	Liver Acquisition with Volume Acceleration (3D LAVA)	28
3.2	Data Analysis for Phantom Imaging	30
3.2.1	Comparison T_1 values of M2D FSPGR, 3D FSPGR and 3D LAVA with FSE-IR	30
3.3	Imaging Experiment on Volunteers	32
3.3.1	M2D FSPGR	30
3.3.2	3D FSPGR	34
3.3.3	3D LAVA	36
3.4	Data Analysis for Volunteers Imaging	39
3.4.1	Comparison of T_1 Values Estimated for Different anatomical orientation	39
3.4.2	Comparison of T_1 Values Estimated for Different Scanning Technique	41
3.4.3	Comparison of T_1 Values Estimated for Different Pulse Sequences	43

CHAPTER 4 DISCUSSION

4.1	Imaging Experiment on Gel Phantoms	46
4.1.1	Fast Spin Echo Inversion Recovery (FSE-IR)	46

4.1.2	Comparison of T_1 Values of 2D FSPGR, 3D FSPGR and LAVA with IR-FSE	46
4.2	Imaging Experiment on Volunteers	48
4.2.1	Comparison of T_1 values of different anatomical orientation	48
4.2.2	Comparison of T_1 values of different scanning technique	48
4.2.3	Comparison of T_1 values of different pulse sequence	49
CHAPTER 5 CONCLUSION		
5.1	Conclusion	50
5.2	Limitation of this study	51
5.3	Recommendation of Future works	52
REFERENCES		53

LIST OF FIGURES

Figures No.		Page
1.1	Spin lattice relaxation time (T_1) is the time taken 63% of M_0 to recover along the z-axis.	5
1.2	Diagram of a spin echo pulse sequence	9
1.3	Diagram of a basic inversion recovery pulse sequence	10
1.4	The diagram of gradient echo pulse	11
1.5	Diagram of 3D gradient echo pulse sequence	14
2.1	The flowchart of the T_1 mapping	19
2.2	The ROIs placed in the centre of the phantom for T_1 measuring	20
2.3	The four ROIs used to determine the average T_1 of fat and muscle tissues	21
3.1	Typical images of gel produced using FSE-IR pulse Sequence with inversion time of (a) 50 ms, (b) 300 ms, (c) 550 ms, (d) 800 ms, and (e) 1050 ms.	22
3.2	Plot of signal intensity as a function of inversion time produced using FSE-IR pulse sequence.	23
3.3	Phantoms images of M2D FSPGR pulse sequence with flip angle of (a) 5° (b) 10° (c) 14° . (d) Image of phantom with T_1 map produced using the three images of (a), (b) and (c).	24
3.4	Images of gel phantoms produced using 3D FSPGR pulse sequence with flip angle of (a) 5° (b) 10° (c) 14° . (d) The T_1 map produced using images of (a), (b) and (c).	26
3.5	Phantoms images of LAVA pulse sequence with flip angle of: (a) 5° (b) 10° (c) 14° . (d) Image of phantom with T_1 map produced using images of (a), (b) and (c).	27
3.6	The T_1 values of gel phantom using differences	

	pulse sequence	28
3.7	Percentage difference of T_1 values at M2D FSPGR, 3D FSPGR and 3D LAVA with respect to FSE-IR pulse sequence	28
3.8	Typical images of volunteer right thigh using M2D FSPGR pulse sequence at axial view with flip angle of (a) 5° (b) 10° (c) 14° . (d) Typical image of volunteer right thigh with T_1 map acquired from the three images (a), (b) and (c).	30
3.9	Typical images of volunteer right thigh using M2D FSPGR pulse sequence at coronal view with flip angle of; (a) 5° (b) 10° (c) 14° . (d) Typical image of volunteer right thigh with T_1 map acquired from images (a), (b) and (c).	31
3.10	Typical images of volunteer right thigh scanned by using 3D FSPGR pulse sequence at axial view with flip angles of; (a) 5° (b) 10° (c) 14° . (d) Typical image of volunteer right thigh with T_1 map acquired from images (a), (b) and (c).	32
3.11	Typical images of volunteer right thigh using 3D FSPGR pulse sequence at coronal view with flip angle of; (a) 5° (b) 10° (c) 14° . (d) Typical image of volunteer right thigh with T_1 map acquired from the three images (a), (b) and (c).	33
3.12	Typical images of volunteer right thigh using 3D LAVA pulse sequence at axial view with flip angle of (a) 5° (b) 10° (c) 14° . (d) Typical image of volunteer right thigh with T_1 map acquired from images (a), (b) and (c).	34
3.13	Typical images of volunteer right thigh using 3D LAVA pulse sequence at coronal view with flip angle of (a) 5° (b) 10° (c) 14° . (d) Typical image of volunteer right thigh with T_1 map acquired from images (a), (b) and (c).	35
3.14	The T_1 values of fat different with difference in anatomical orientation for three pulse sequence	36
3.15	The T_1 values of muscle different with difference in anatomical orientation for three pulse sequence	37
3.16	The T_1 values of fat different with difference in scanning technique for FSPGR pulse sequence	38
3.17	The T_1 values of muscle different with difference in scanning technique for FSPGR pulse sequence	39

3.18	The T_1 values of fat different with difference pulse sequence for two orientations	41
3.19	The T_1 values of muscle different with difference pulse sequence for two orientations	42

LIST OF TABLES

Tables No.		Page
1.1	T ₁ value for fat and muscle from literature	4
2.1	Concentration of GdCl ₃ in the gel phantoms	15
2.2	Scanning parameters setup for gadolinium gel phantoms	17
2.3	Scanning parameters setup for volunteers	21
3.1	T ₁ values of gel phantoms using FSE-IR pulse sequence	23
3.2	T ₁ values of gel phantoms using M2D FSPGR pulse sequence	25
3.3	T ₁ values of gel phantoms using 3D FSPGR pulse sequence	26
3.4	T ₁ values of gel phantoms using 3D LAVA pulse sequence	27
3.5	The percentage difference of T ₁ values respect to FSE-IR pulse sequence.	29
3.6	T ₁ values of fat and muscle by using M2D FSPGR pulse sequence at axial and coronal orientation.	32
3.7	T ₁ values of fat and muscle by using 3D FSPGR pulse sequence at axial and coronal orientation.	34
3.8	T ₁ values of fat and muscle by using 3D LAVA pulse sequence at axial and coronal orientation	36
3.9	The percentage difference of T ₁ values for difference scanning orientation for three pulse sequences	38
3.10	The percentage difference of T ₁ values for difference dimensional of scanning technique with respect to 3D FSPGR	40
3.11	The percentage difference of T ₁ values for 3D LAVA with respect to 3D FSPGR pulse sequence	43

LIST OF EQUATION

Equation No.		Page
1.1	Linear Relationship of signal intensity and contrast agent concentration	6
1.2	Standard Toft model	7
1.3	Relationship of v_e and K^{trans}	7
2.1	Spin Echo (SE) Equation	17
2.2	Gradient echo (GE) Equation	18
3.1	Percentage Difference for Difference Pulse Sequence for phantom Equation	28
3.2	Percentage Difference for Difference Scanning Orientation Equation	37
3.3	Percentage Difference for Difference Dimensional of pulse Sequence Equation	40
3.4	Percentage Difference for difference pulse sequence Equation	42

LIST OF APPENDICES

Appendix No.		Page
Appendix A		
Appendix A(i)	Ethic approval form from Ethical Committee UMMC	56
Appendix A(ii)	Sample of consent form given to volunteers	58
Appendix B		
Appendix B (i)	T ₁ value measurement for phantoms using M2D FSPGR	59
Appendix B (ii)	T ₁ value measurement for phantoms using 3D FSPGR	59
Appendix B (iii)	T ₁ value measurement for phantoms using 3D LAVA	59
Appendix C		
Appendix C (i)	T ₁ value of muscle measurement for volunteer using M2D FSPGR, 3D FSPGR and 3D LAVA	60
Appendix C (ii)	T ₁ value of fat measurement for phantoms using M2D FSPGR, 3D FSPGR and 3D LAVA	60

LIST OF SYMBOLS, ABBREVIATIONS OR NOMENCLATURE

MRI	Magnetic resonance imaging
RF	Radio frequency
CT	Computed tomography
FOV	Field-of-view
T_1	spin-lattice relaxation
T_2	spin-spin relaxation
PD	Proton density
BOLD	Blood oxygenation level dependent
DWI	Diffusion weighted imaging
DCE-MRI	Dynamic contrast enhanced-magnetic resonance imaging
Gd-DTPA	Gadolinium diethylenetriaminepentacetate
EES	Extracellular extravascular space
k^{trans}	Transfer constant
v_e	Total EES volume
IR	Inversion recovery
TI	Inversion time
FSE-IR	Fast Spin Echo Inversion Recovery
FSPGR	Fast SPoiled GRadient echo
FLASH	Fast Low Angle Shot
LAVA	Liver Acceleration of Volume Acquisition
GE	General Electronic
M_z	Longitudinal magnetization
MR	Magnetic resonance
S	Signal intensity procontrast
S_0	Signal intensity precontrast
Gd	Gadolinium

GSS	Slice selection gradient
TE	Echo time
GPE	Phase encoding gradient
GFE	Frequency encoding
STIR	Short TI Inversion Recovery
CSF	Cerebrospinal fluid
FLAIR	FLuid Attenuated Inversion Recovery
FID	free induction decay
TR	repetition time
2D	Two dimensional
3D	Three dimensional
SNR	Signal to noise ratio
GdCl ₃	Gadolinium (III) chloride
ms	milliseconds
mm	millimetre
kHz	kilo Hertz
ROI	Regions of interest
M2D	Multislices 2D

CHAPTER 1

INTRODUCTION

1.1 Background

Magnetic resonance imaging (MRI) is one of the most widely used imaging methods to diagnose diseases. The machine employs magnetic and radiofrequency (RF) fields, which are non-ionizing radiations. Hence, it is considered much safer to the patient compared to X-ray based imaging modalities such as X-ray fluoroscopy and computed tomography (CT). MRI acquires signals from atomic nuclei, particularly hydrogen protons, which are abundant in human body (Dhawan, 2011). The MR signals are normally acquired when the protons are returning (or relaxing) to their equilibrium conditions from their excited states. Only protons in a preselected slice or volume are excited and then spatially encoded to form images. These processes are performed by using gradient coils, which create position dependent field strengths in the field-of-view (FOV).

One of the main advantages of MRI compared to other imaging modalities is it is able to produce images based on a variety of contrast mechanisms. The most basic and common image contrasts used in clinical imaging are spin-lattice (T_1)-weighted, spin-spin (T_2)-weighted and proton density (PD)-weighted images. Different image weighted technique has different diagnostic application. For example, the T_1 -weighted images have

excellent tissue contrast and also called anatomy scan because of its ability to produce an excellent contrast between different tissues. The T_2 -weighted technique is also called pathology scan because of its ability to produce higher signal intensity in pathology than the normal tissue. The PD-weighted technique is based on the density of hydrogen protons or water content in the tissues. This technique is normally used in musculoskeletal studies for example to distinguish between articular cartilage from the cortical bone and menisci in the knee (McRobbie et al., 2007). Other than the three basic MRI pulse sequences, there are many other MRI techniques that have been developed by MR researchers such as blood oxygenation level dependent (BOLD), diffusion weighted imaging (DWI) and dynamic contrast-enhanced (DCE)-MRI.

In this study, I focused on the T_1 measurement techniques, which is one of the steps required in quantitative DCE-MRI studies. DCE-MRI is used to evaluate vascular characteristic of tumours such as blood volume, vascular leakage space and vascular permeability. The technique employs contrast agent i.e. gadolinium diethylenetriaminepentaacetate (Gd-DTPA) which is used to enhance the appearance of tumours in tissues. Different imaging techniques may affect the accuracy of T_1 values measured. Hence, the accuracy of the T_1 values measured will also affect the quantitative parameters determined by using quantitative DCE-MRI such as transfer constant from the blood plasma into the extracellular extravascular space (K^{trans}) and total extracellular extravascular space (EES) volume (v_e).

1.2 Objectives

The aims of this research project are:

- a) To develop the T_1 mapping technique for DCE-MRI application
- b) To compare the accuracy of T_1 mapping produced using different MRI pulse sequences
- c) To evaluate the T_1 mapping using different imaging techniques in volunteers

1.3 Literature review

T_1 values have several applications in MRI such as to optimize MRI protocols in clinical imaging and to estimate contrast agent uptake in the tissues. Different techniques can be used to measure T_1 values in the tissue. The standard technique used is based on inversion recovery (IR) pulse sequences. By using this technique, a few set of images acquired by using different inversion time (TI). The T_1 values are estimated by fitting the curve of signal intensities versus TI. Rakow-Penner et al. employed a modified IR technique to determine the T_1 value called IDEAL. IDEAL imaging discovered the partial volume effects of fat and glandular tissue on quantifying relaxation rates of independent tissue types. By using IDEAL sequence, a precise measurement of T_1 in fat and fibroglandular tissue can be made. The main drawback of the inversion recovery technique is it is time consuming to be performed in clinical imaging.

An alternative technique to measure T_1 which is commonly used in clinical imaging is a variable flip angle by using spoiled gradient echo pulse sequence. This technique is performed by acquiring a few sets of gradient echo images each one with different flip angle settings. The T_1 values are then determined by fitting the curve of signal intensities as a function of flip angles (Brookes et al., 1999; W.Lin & Song, 2009). Combination of two to four flip angles is commonly used for this purpose (Brookes et al., 1999; W.Lin & Song,

2009). Table 1.1 shows example of T_1 values using 1.5 Tesla MRI scanners reported in the literature.

Table 1.1: The T_1 value for fat and muscle at 1.5 Tesla from literature

References	T_1 value for fat (ms)	T_1 value for muscle (ms)
Brookes et al. (1999)	240 (Breast fat)	-
Rakow-Penner et al. (2006)	372.04 (Breast fat)	-
de Bazelaire et al. (2004)	343	856
Han et al. (2003)	288 (Subcutaneous fat)	1130 (Knee)
Moore (2005)	200	1075
Bushberg et al. (2002)	260	870
Nitz et al. (2010)	-	868

1.4 Theory

1.4.1 Spin-lattice relaxation (T_1)

Spin-lattice or longitudinal relaxation time (T_1) is an intrinsic property of a tissue which is dependent on the mobility of protons and molecular structure and chemistry of tissues (Kirsch, 1991). Different tissues may have different T_1 values compared to other tissue. The parameter can be characterized by the time constant for protons to align themselves with the external magnetic field from the excited state. For example, after a 90° RF excitation pulse, the T_1 is given by the time required for a longitudinal magnetization (M_z) to recover to 63% of its maximum value (see figure 1.1). T_1 values are dependent on the external magnetic field strength. The values increase with the field strength of an MRI machine (Rakow-Penner et al., 2006).

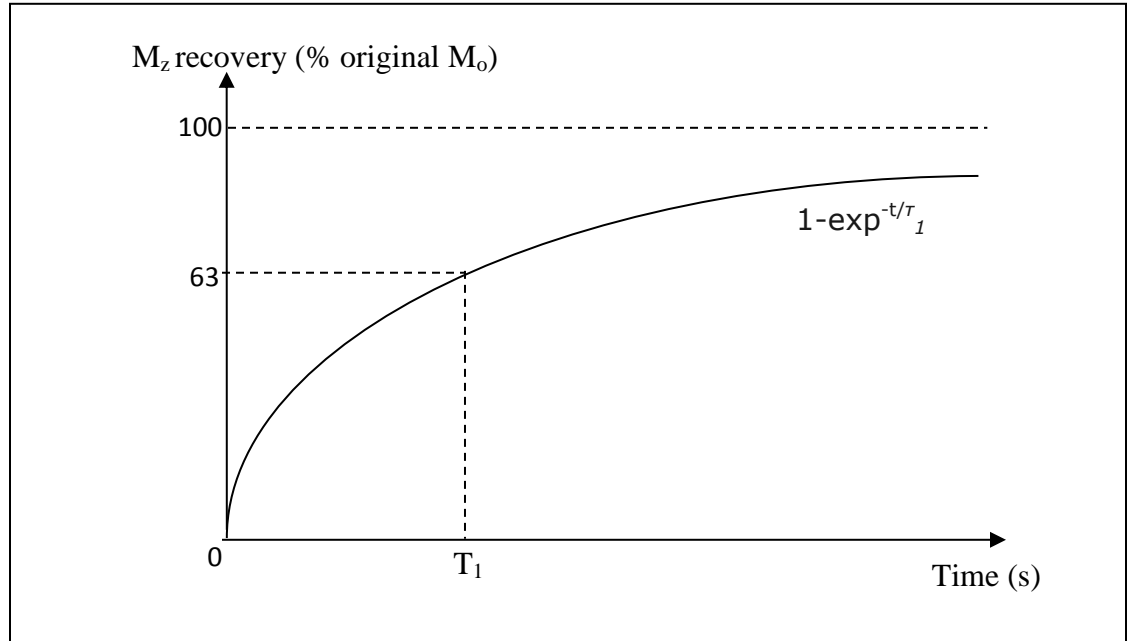


Figure 1.1: Spin lattice relaxation time (T_1) can be defined as the time taken for a longitudinal magnetization (M_z) to recover to 63% of its maximum level (M_0) after a 90° RF excitation.

The signal intensity of a T_1 weighted image is not only determined by the T_1 of a tissue but it also partially contributed by other parameters such as T_2 and proton density. A quantitative T_1 image (T_1 map) can be produced by fitting signal intensities of images acquired with different settings such as TI and flip angle (α) to the related equation.

1.4.2 DCE-MRI

DCE-MRI is considered as one of the most sensitive technique to diagnose cancers especially in the breast (Brookes et al., 1999; Rakow-Penner et al., 2006). It is performed by administering a Gd-DTPA contrast agent into the patient. The distribution of contrast

agent within the tissues is monitored by using a fast MRI technique such as Fast SPOiled GRAdient echo (FSPGR), Fast Low Angle Shot (FLASH) and Liver Acceleration of Volume Acquisition (LAVA) pulse sequences. The measurement of native T_1 value of tissue is required in quantitative (pharmacokinetic based) DCE-MRI to quantify the concentration of contrast agent from signal intensity in the dynamic images acquired. Brooke et al. (1999) suggested that quantifying signal enhancement without taking account the T_1 of particular tissue displaying enhancement might be a cause of reduced specificity. The relationship of signal intensity and the contrast agent concentration (linear relation is assumed) is given by Eq. [1.1] by Henderson et al. (2000):

$$\frac{S-S_0}{S_0} \approx T_{10}r[Gd] \quad [1.1]$$

where S is post-contrast signal intensity i.e signal intensities of dynamic images acquired after injection of contrast agent, S_0 is pre-contrast signal intensity i.e. signal intensities of image acquired before the injection of contrast medium, T_{10} is a native T_1 value (T_1 of tissues before contrast administration), r is a constant which represents the relaxivity i.e. the ability of a paramagnetic species to influence relaxation rates (Higgins et al.,1987) of the contrast agent and $[Gd]$ is the concentration of gadolinium contrast agent. Eq. [1.1] shows the contrast agent concentration can be estimated if T_{10} is known (Buckley et al., 2005). Hitmair et al. (1994) suggested that the specificity of DCE-MRI can be improved if the concentration of contrast agent taken up by a tissue is known. Using the standard Tofts model (Tofts, 1997), contrast agent uptake can be approximated using Eq. [1.2]:

$$C_t(t) = \frac{K^{trans}}{1-Hct} (C_a(t) \otimes e^{k_{ep}(t-z)}) \quad [1.2]$$

where $C_t(t)$ represents tissue concentration as a function of time, K^{trans} is transfer constant from the blood plasma into the extracellular extravascular space (EES), Hct is the haematocrit value, $C_a(t)$ represents arterial concentration as a function of time, k_{ep} is transfer constant from the EES back to the blood plasma, t represents onset time of arterial contrast uptake. Total EES volume (v_e) can be determined by using Eq. [1.3]:

$$v_e = \frac{K^{trans}}{k_{ep}} \quad [1.3]$$

The concentration of contrast agent from Eq. [1.1] represents the tissue concentration in the Eq. [1.2]. Therefore, errors in the T_1 values measured will reduce the accuracy of pharmacokinetic parameters such as k^{trans} and v_e estimated by using Eq. [1.2].

1.4.3 Magnetic Resonance Imaging (MRI) pulse sequence

MRI is one of the most flexible imaging techniques available. Different image properties such as T_1 -weighted and T_2 -weighted can be produced by using different combination, strength and timing of RF and gradient pulses applied during imaging. This repeating application of pulses is called pulse sequence. In general, MRI pulse sequences can be grouped into two types: spin echo pulse sequence and gradient echo pulse sequence.

1.4.3.1 Spin echo pulse sequence

The spin echo pulse sequence employs a 90° excitation RF pulse followed by a 180° refocusing RF pulse at half the time-to-echo (TE) to create an echo. A slice selection

gradient (SSG) is normally applied at the same time as the RF pulse to excite a desired slice thickness or a slab at a specific position along the patient. A 'negative' gradient is applied immediately after the SSG in the slice selective direction to compensate the dephasing of generated transverse magnetization occurred because of the frequency difference during the excitation process. The frequency encoding (FEG) or readout gradient is applied to collect the MR signal. The phase encoding gradient (PEG) is applied between the SSG and PEG so that the information of the third dimension is encoded into the echo. Figure 1.2 shows a typical spin echo pulse sequence.

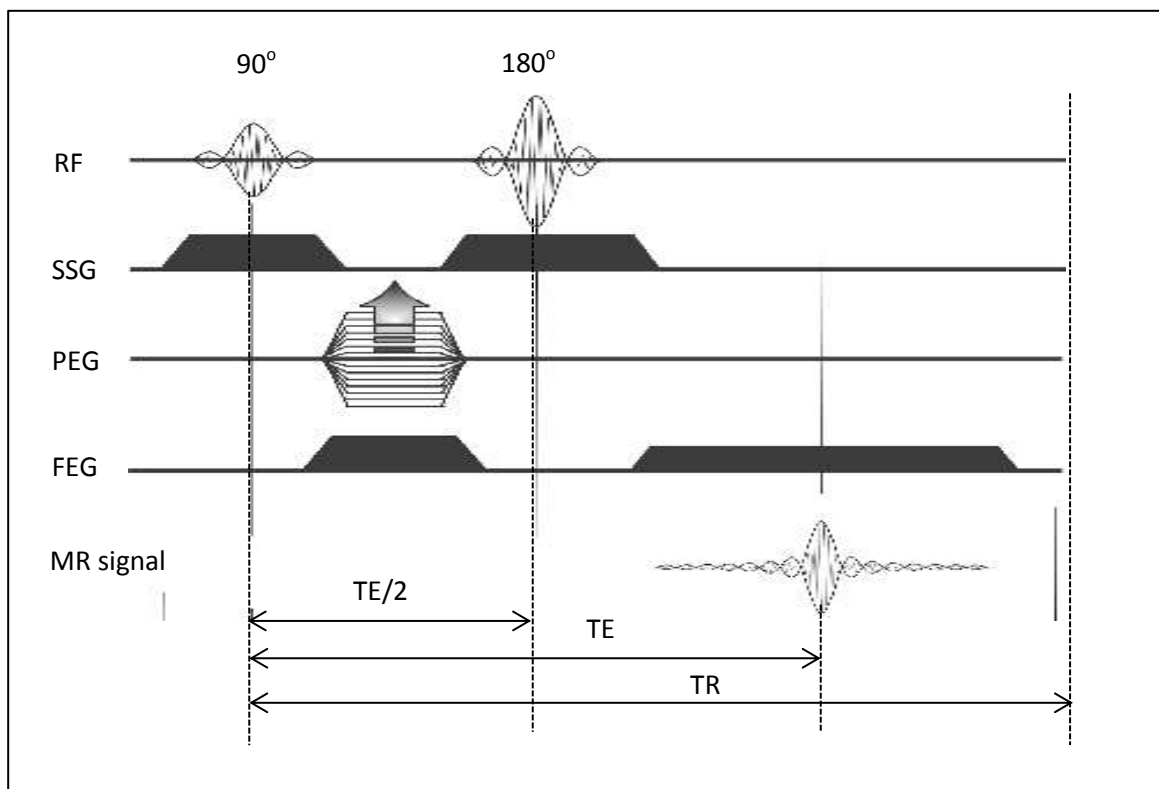


Figure 1.2: Diagram of a spin echo pulse sequence adopted from Nitz et al. Spin echo pulse sequence uses an initial 90° excitation RF pulse followed by a 180° refocusing pulse after a delay time equal to $TE/2$ to invert the spins and produces an echo at time TE . The gradient slice was applied on slice selection. The gradient phase was applied immediately after the gradient slice to compensate the dephasing of generated transverse magnetization. The readout gradient is applied to collect MR signal.

1.4.3.1.1 Fast Spin Echo Inversion Recovery (FSE-IR)

Inversion recovery sequence is commonly performed by applying a slice selective 180° degree RF pulse before the spin echo pulses i.e. 90° and 180° pulses (Figure 1.3). The duration between the inversion pulse and the 90° RF pulse is called time-to-invert (TI). Like the normal spin echo, a 180° degree RF pulse is applied at half the TE to create an echo. Inversion recovery pulse sequences with a very short TE can produce a heavy T_1 -weighting in the signal.

In clinical imaging, normally a faster version of IR technique i.e. fast spin echo inversion recovery (FSE-IR) is normally used. In this pulse sequence, more than one 180° refocusing pulse are applied after the 90° excitation pulse. Hence, more than one echo are generated from one RF excitation. For clinical application, this pulse sequence is usually used as Short TI Inversion Recovery (STIR) or FLuid Attenuated Inversion Recovery (FLAIR). In STIR, a short TI is used to eliminate the fat signal, a long TI is used in FLAIR to saturate signal from cerebrospinal fluid (CSF) (McRobbie et al., 2007).

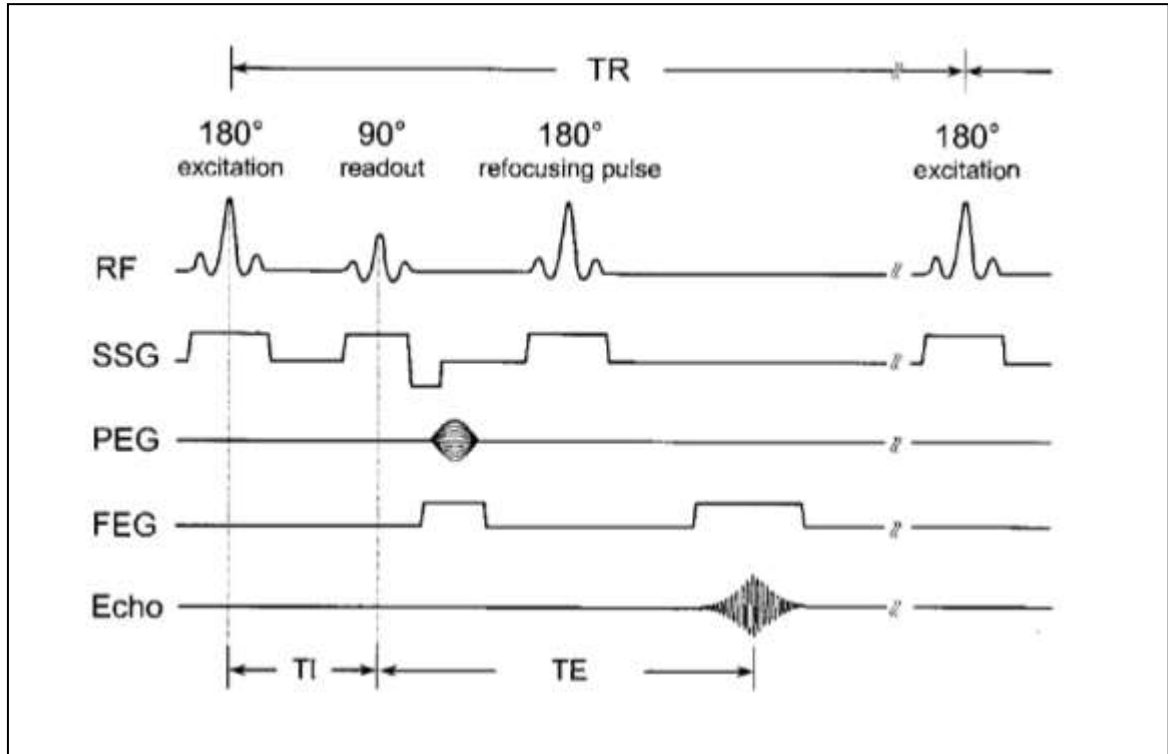


Figure 1.3: Diagram of a basic inversion recovery pulse sequence (Bushberg et al., 2002). Inversion recovery pulse sequence apply an initial 180° RF pulse and followed by 90° RF pulse after inversion time (TI) and then apply with second 180° RF pulse at a time TE/2. The SSG is applied to localize the spins in the desired plane.

1.4.3.2 Gradient Echo Pulse Sequences

In gradient echo technique, an RF pulse with flip angle of less than 90° is normally used. The echo is generated by using gradient fields instead of 180° RF pulses in the frequency encode direction. The gradient field has two lobes where the first ('negative') lobe is in opposite direction and half of the size of the second lobe of the gradient field. The 'negative' lobe is used to dephase the transverse magnetization before the signal readout. Hence, the spins will be in phase at the center of the readout gradient. Like the spin echo, PEG is also applied between the SSG and FEG.

The gradient echo pulse sequences are sensitive to susceptibility difference between different tissues or medium especially at bone-tissue or air-tissue interfaces. This often lead to an overall signal loss in the surrounding area of these particular regions. However, this effect can be useful in some clinical application such as in imaging of haemorrhagic lesions and perfusion studies.

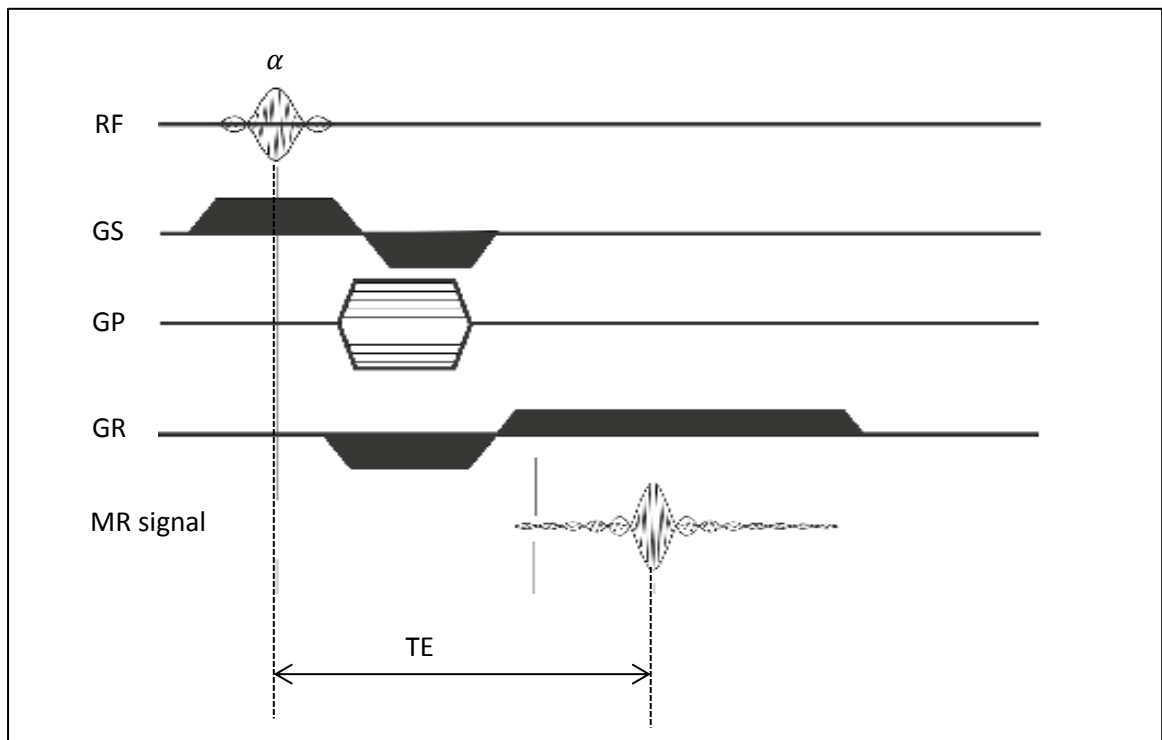


Figure 1.4: A diagram of a typical gradient echo pulse sequence adapted from Nitz et al. gradient echo pulse sequence uses an initial RF pulse with flip angle (α) of less than 90° . The echo is generated by using gradient fields in the frequency encode direction.

1.4.3.2.1 Fast Spoiled Gradient echo (FSPGR)

A Fast SPoiled GRAdient echo (FSPGR) is based on the gradient echo technique. In this sequence, a low flip angle (10° to 60° degree) of RF pulses is used to excite the protons (Nitz et al., 2010). The transverse magnetization is spoiled after the signal readout by using RF or gradient spoiling techniques. Other gradient fields used are similar to the standard gradient echo pulse sequence. To produce a T_1 -weighted image, a large flip angle with a short repetition time (TR) and short echo time (TE) are applied.

1.4.3.2.2 Liver Acceleration of Volume Acquisition (LAVA) Pulse Sequence

The LAVA pulse sequence is based on the 3D FSPGR pulse sequence. In its standard form, a fat suppression is automatically applied. However, this function can be deactivated in the MRI machine. In this pulse sequence, a very short TR and TE are applied, which is useful to allow a very fast imaging time. This technique is very useful in abdominal imaging by providing a high spatial and temporal resolution images with good fat suppression and also in dynamic imaging (Low et al. 2010).

1.4.4 2D versus 3D Image Acquisition

Two-dimensional (2D) image acquisition is the technique of MRI scanning defined by a selective excitation. The thickness of the slice in 2D acquisition is limited by the gradient strength, the Fourier transform of the RF pulse profile, and the excitation bandwidth. Furthermore, because of imperfections in the excitation pulse, gaps are left between slices to avoid signal loss and altered image contrast. The 2D and 3D image have

similar resolution when viewing as a plane, but different geometric while viewed in the slice direction (Higgins et al., 1987).

3D acquisition methods encode slices with phase-encoding gradients in a manner similar to that of in-plane phase encoding. Because the slice selection gradient is not used to encode slices, there is no practical limit on of the slice thickness. Slice thickness in 3D studies can be made that approximate in-plane resolution. The data from 3D study can be viewed in any desired direction without a perceptible loss in resolution (Higgins et al., 1987).

In clinical imaging, normally the images are acquired using a multislice 2D or 3D technique. In the conventional multislice 2D technique, the slice selection is performed sequentially i.e. the second slice only will be excited after all the signals acquired to produce an image slice are collected. To reduce the scanning time in multislice 2D technique, an interleave technique is commonly used. By using this technique, the scanner excited the other slices by changing the central frequency of the RF pulse in the object during the TR period of the first slices. Thus, during each TR the scanner excites and collects the echoes from many slices (McRobbie et al., 2007).

In the multislice 2D, the spacing between slices is normally kept to a small space so that small pathologies that lie between the gaps will not be missed. However, too small slice gap may cause crosstalk i.e. the signals of difference slices to mix with each other. This is due to the imperfect rectangular shape of the profile in each slice.

In a standard 3D image acquisition technique an additional second phase-encode gradient is applied in the slice selective direction. A selective RF pulse excites spins in a slab (volume) of the subject instead of a thin slice as in the 2D technique. In this technique phase encoding is applied in two directions i.e. in phase encoding gradient and in slice (slab) selective direction (figure 1.5).

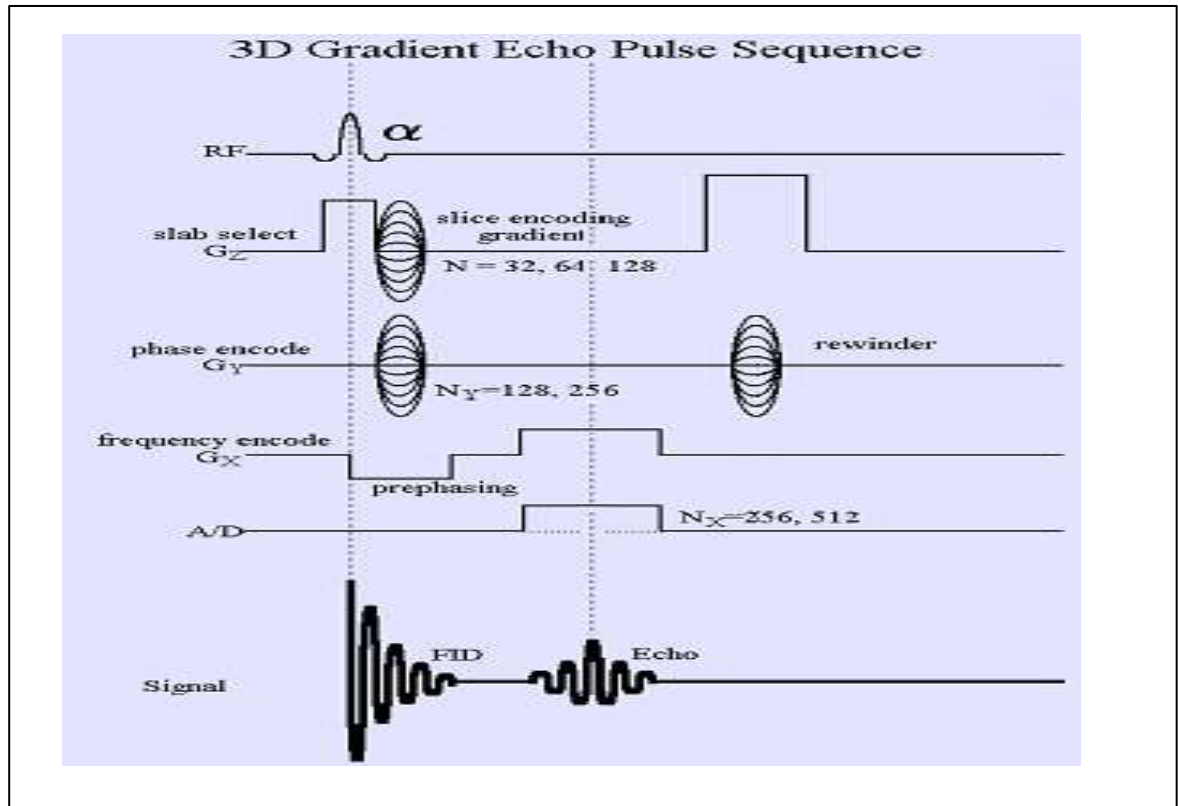


Figure 1.5: Diagram of 3D gradient echo pulse sequence (Allison et al., 2010). 3D gradient echo pulse sequence basically similar to conventional gradient echo pulse sequence but in 3D pulse sequence phase encoding gradient were applied in slab selection direction.

The 3D technique is normally used to produce high resolution images with thin slices. It allows a higher number of slices with more rectangular profile and signal to noise ratio (SNR) for an equivalent slice thickness acquired by using a 2D technique. However,

the main drawback of the technique is it requires a long acquisition time. Furthermore, ringing and aliasing artefact from neighbouring slices are more common in this technique compared to the 2D method.

The slice profiles over the central slices of an image data set acquired with 3D sequence may be assumed to be rectangular; this assumption is invalid for 2D slices, where the individual slice profiles will be nonrectangular (Hänicke et al., 1988).

CHAPTER 2

METHODOLOGY

2.1 Imaging Experiment on Gel phantoms

Imaging experiments were performed on T_1 gel phantoms by using a GE 1.5 Tesla MRI system (Signa HDx, General Electric Healthcare, USA). The gel phantoms used in this study was constructed by Mr. C.K Chia and Ms. Y.H. Lin (Lin, 2012), former students of Master Medical Physics Program, University of Malaya. The gel phantoms were constructed from gadolinium (III) chloride ($GdCl_3$). Different concentration of $GdCl_3$ was used to produce seven phantoms with different T_1 value. The concentration of $GdCl_3$ is given in table 2.1. Gadolinium is a paramagnetic contrast agent used in MRI. Gadolinium has seven unpaired electrons which contribute its strong paramagnetic property (Raymond et al., 2005). The material will change signal intensities in the T_1 -weighted image by shortening T_1 value of the surrounding protons within water molecules.

Table 2.1: The concentration of $GdCl_3$ in the gel phantoms adapted from Lin (2012).

Phantom	Concentration of $GdCl_3$ (M)
A	1.450
B	0.689
C	0.435
D	0.182

E	0.098
F	0.056
G	0.030

The gel phantoms were placed horizontally in between a pair of cardiac RF coils. The phantoms were placed at the same positions during image acquisition. The experiments were performed by using four different pulse sequences; i.e. FSE-IR, M2D FSPGR, 3D FSPGR and 3D LAVA.

An FSE-IR pulse sequence technique was performed to measure the T_1 values on the gadolinium gel phantoms. This technique is considered as the standard method in the measurements of T_1 . However it is not routinely used for *in vivo* imaging because it is time consuming to be performed in clinical setting. The T_1 relaxation time was measured by using FSE-IR preparation with different setting of TI. A repetition time (TR) of 6500 ms and echo time (TE) of 7.51 ms were used. Images were acquired with this following TI values: 50, 300, 500, 800 and 1050 ms to determine the value of T_1 more accurately because the T_1 value estimated from the graph fitted by signal intensity and TI values.

The second imaging technique used was axial M2D FSPGR sequence with flip angles of 5° , 10° and 14° , TR of 9.1 ms, TE of 1.75 ms. The third technique was axial 3D FSPGR sequence with flip angles of 5° , 10° and 14° , TR of 11.61 ms and TE of 5.26 ms. The fourth technique was axial 3D LAVA pulse sequence with flip angles of 5° , 10° and 14° , TR of 5.27 ms and TE of 2.62 ms. Parameter settings used are summarized in table 2.2.

Table 2.2: Scanning parameters used in imaging experiment on T₁ gel phantoms

Parameters	M2D FSPGR	3D FSPGR	LAVA	FSE-IR
Repetition time (ms)	9.1	11.61	5.27	6500
Echo time (ms)	1.75	5.26	2.62	7.51
Flip angle (α)		5°, 10°, 14°		-
Inversion time (ms)	-	-	-	50, 300, 550, 800, 1050
No of slices	5	44	44	1
Slices thickness (mm)	5	3	3	5
Echo train length	1	1	1	7
Field of view (mm)	220	220	220	220
Image size (pixel)	512 × 512	256 × 256	512 × 512	256 × 256

2.1.1 Image Analysis of Experiments on gel Phantoms

Signal intensity was measured from circular regions-of-interest (ROI) drawn over each DICOM images of gel phantoms using ImageJ 1.43u (National Institute of Health, USA) software for FSE-IR. Graphs of signal intensity versus IR were plotted using Matlab (MathWorks, Natick MA). Matlab's Curve fitting function were used to determine the value of T₁ from combination of five different TI for FSE-IR pulse sequence. The T₁ values were determined from the curve fitting are based on the equation Eq. [2.1] (Bushberg et al. 2002, McRobbie et al., 2007).

$$S = S_0 \left[1 - 2e^{-\frac{TI}{T_1}} \right] \quad [2.1]$$

where S represents the signal intensity of the image and S_0 represents the maximum signal intensity at equilibrium condition.

Since the M2D FSPGR, 3D FSPGR and 3D LAVA are based on spoiled gradient echo pulse sequence (McRobbie et al., 2007), the same equation, Eq. [2.2] was used for curve fitting process. For this equation the flip angle (α) is the manipulating factor. The flip angle used in this experiment was 5° , 10° and 14° . Other parameters including TR and TE were fixed.

$$S = M_0 \frac{\left[1 - e^{-\frac{TR}{T_1}}\right] \sin \alpha}{1 - \left[e^{-\frac{TR}{T_1}}\right] \cos \alpha} \quad [2.2]$$

where S is the signal intensity obtains from the image and M_0 is the magnetization at equilibrium condition.

For the spoiled gradient echo based sequences, the T_1 values were displayed as T_1 map. The map was produced by calculating the T_1 values by curve fitting technique for each pixel in the image. The mapping is performed by uploading the images with different flip angles into the computer. The image size then reduced from 512×512 pixels to 128×128 pixels. This step is performed to reduce the processing time and to reduce the noise in the T_1 map. After all the imaging parameter setting such as α and TR were set, curve fitting is performed on each pixel in the uploaded image to determine the T_1 values. The value of T_1 then shown as a colour map. The image is then increased back to 512×512 for display purpose. A summary of the techniques used to produce the T_1 map is shown in Figure 2.1.

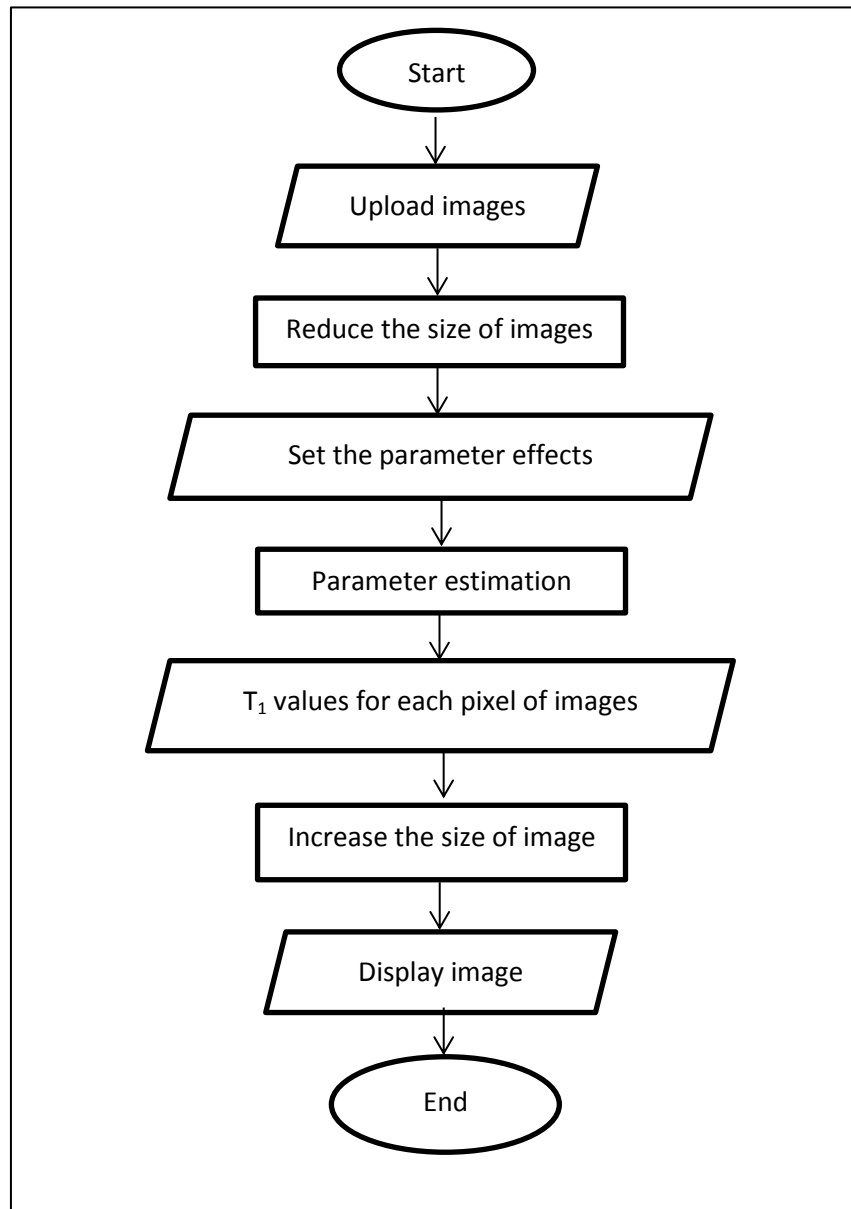


Figure 2.1: The flowchart of the T₁ mapping

The three ROIs were drawn at the centre of phantom with T_1 map produced from mapping technique to measure the average value of the T_1 in each phantom (see figure 2.2).

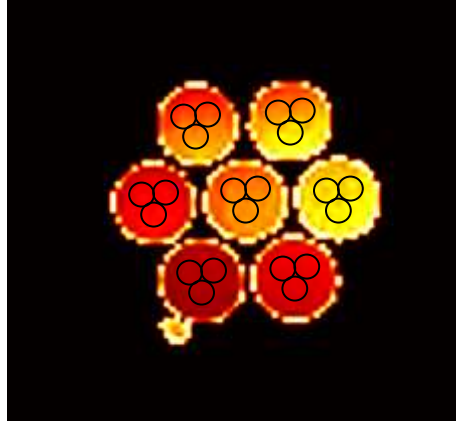


Figure 2.2: Typical image of three ROIs placed at centre of the phantom for T_1 measuring at M2D FSPGR pulse sequence (TR: 9.1 ms; TE: 1.75 ms).

2.2 Imaging Experiment on Volunteers.

Imaging experiment was performed on four healthy volunteers (one male and three female) by using a GE 1.5 Tesla MRI system. Ethical committee approvals were obtained from local ethic committee (Medical Ethics Committee University Malaya Medical Centre) and informed consent was obtained from all the volunteers. The volunteers were positioned prone in the scanner and the cardiac receiver coil was used. The imaging procedures were performed on the right thigh of the volunteer in order to evaluate the value of T_1 of subcutaneous fat and muscle.

The imaging protocol acquires axial and coronal M2D FSPGR images with different flip angles. The experiments were repeated by using axial and coronal 3D FSPGR sequence, followed by axial and coronal 3D LAVA sequence. The 3D LAVA sequence used in this experiment was not the standard from the manufactured which includes the fat suppression in the technique. In this experiment, the fat suppression function of the 3D LAVA pulse sequence was removed to obtain the fat images for data analysis. Flip angles of 5° , 10° and 14° were used in all pulse sequence. Other parameter settings are shown in table 2.3.

Table 2.3: Scanning parameters setup for volunteer

Parameters	2D FSPGR		3D FSPGR		LAVA	
	Axial	Coronal	Axial	Coronal	Axial	Coronal
Repetition time (ms)	9.1	9.1	11.52	11.43	4.91	4.14
Flip angle (α)	$5^\circ, 10^\circ, 14^\circ$					
Echo time (ms)	1.76	1.77	5.18	5.1	2.47	2.03
No of Slices	5	4	60	96	60	116
Slices thickness (mm)	5	5	3	3	3	3
Field of View (mm)	220	270	220	330	220	270
Image size (pixel)	512×512	512×512	256×256	256×256	512×512	256×256

2.2.1 Volunteer Image Analysis

The same technique was used to produce the T_1 map on a volunteer. However, in the volunteer, four ROIs were placed at fat and muscle area (see figure 2.3) to determine the average T_1 of the tissues.

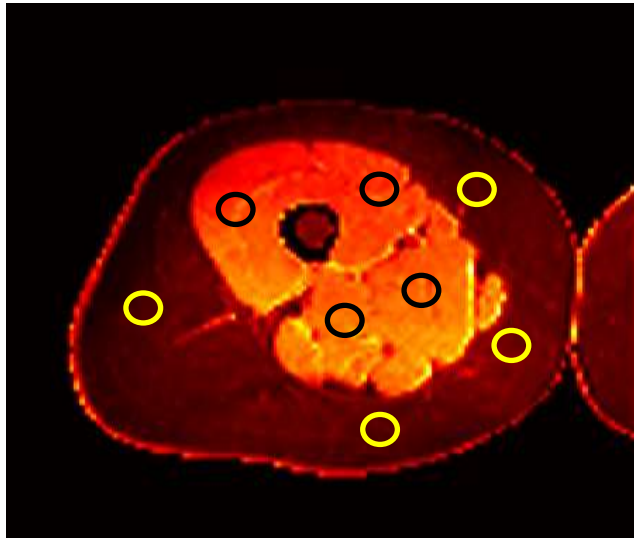


Figure 2.3: Typical image of four ROIs used to determine the average T_1 of fat and muscle tissues at 3D pulse sequence (TR: 11.52 ms; TE: 5.18 ms) at axial orientation.

CHAPTER 3

RESULTS

3.1 Imaging Experiment on Gel Phantom

3.1.1 Fast Spin Echo Inversion Recovery (FSE-IR)

Figure 3.1 shows a set of gel phantom images acquired using different inversion time: 50, 300, 550, 800 and 1050 ms.

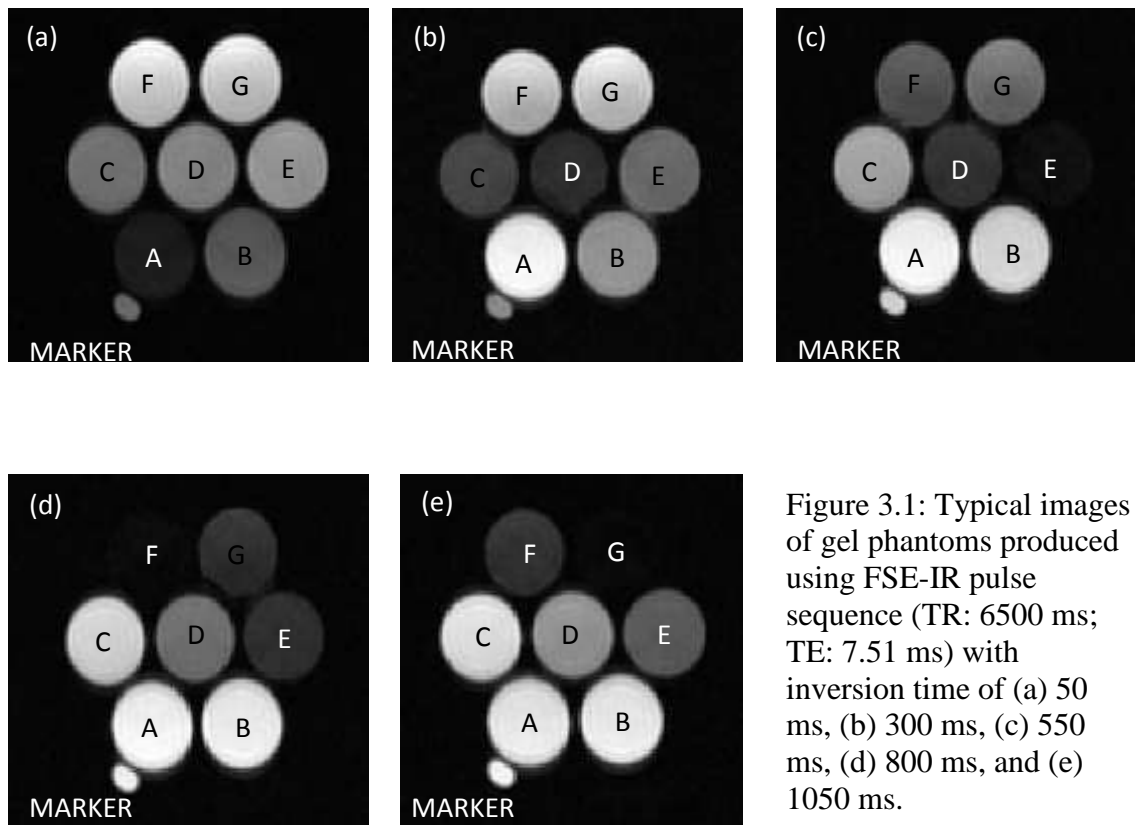


Figure 3.1: Typical images of gel phantoms produced using FSE-IR pulse sequence (TR: 6500 ms; TE: 7.51 ms) with inversion time of (a) 50 ms, (b) 300 ms, (c) 550 ms, (d) 800 ms, and (e) 1050 ms.

Figure 3.2 shows the signal intensity as a function of inversion time for each sample with their respective fitted curves. The T_1 values estimated are given in table 3.1.

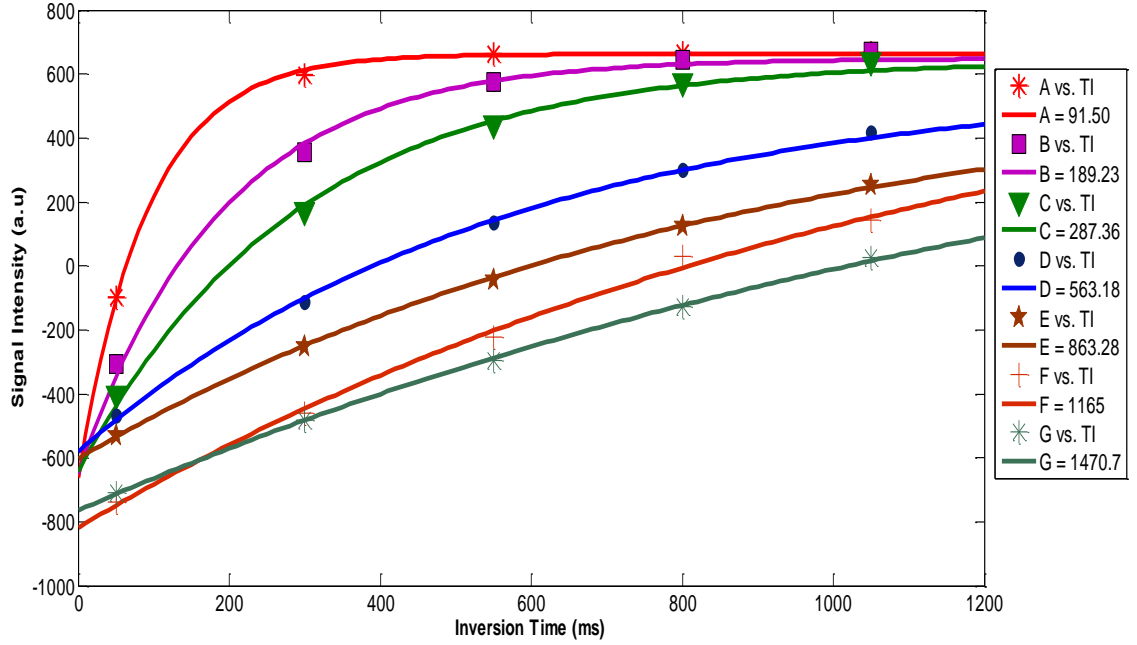


Figure 3.2: Plot of signal intensity as a function of inversion time produced using FSE-IR pulse sequence. All phantoms exhibited different T_1 values are distinguishable from each other at any points of inversion time.

Table 3.1: T_1 values of gel phantoms using FSE-IR pulse sequence acquired from the curve fitting process.

Phantom	T_1 (ms)
A	92
B	189
C	287
D	563
E	863
F	1165
G	1471

3.1.2 Multislices 2D FSPGR (M2D FSPGR)

Figure 3.3(a) to (c) shows images of gel phantoms produced by using M2D FSPGR pulse sequence with three different flip angles (5° , 10° and 14°). Figure 3.3(d) shows the image of T_1 map produced from the three previous images. The colour scale beside the phantoms represents the T_1 values estimated. The T_1 values estimated from each phantom are given in table 3.2.

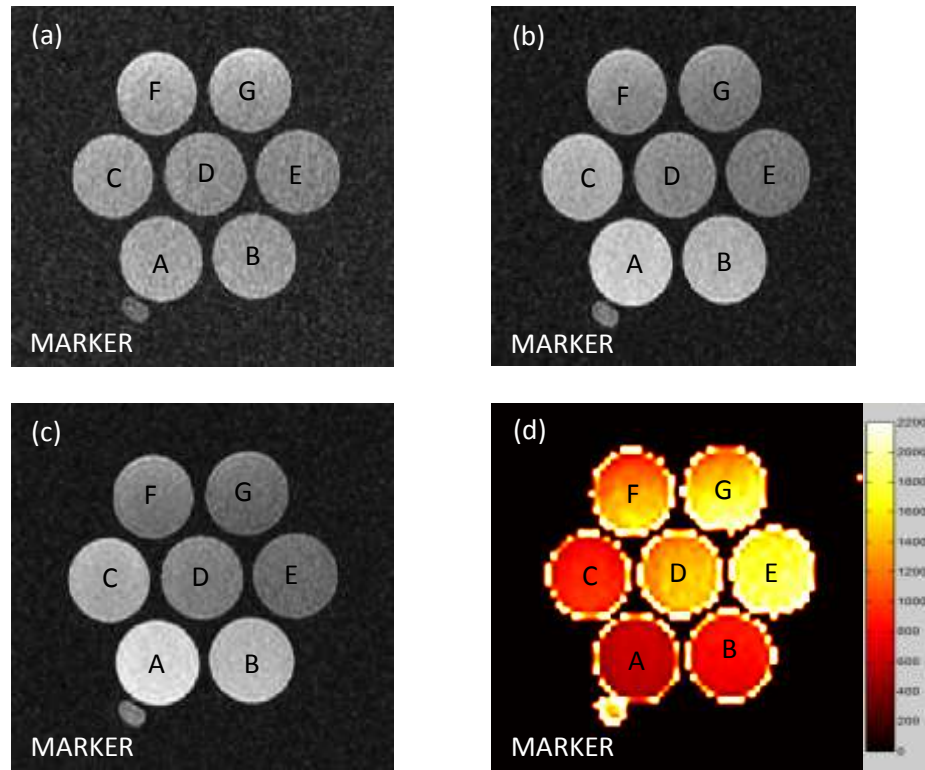


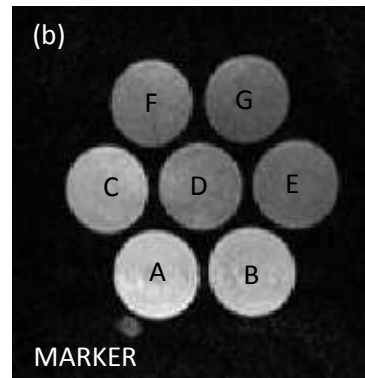
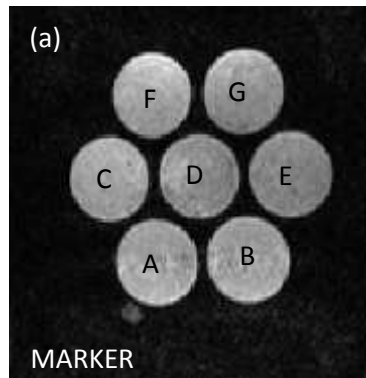
Figure 3.3: Phantoms images of M2D FSPGR pulse sequence (TR: 9.1 ms; TE: 1.75 ms) with flip angle of (a) 5° (b) 10° (c) 14° . Image of phantom with T_1 map (d) produced using the three images of (a), (b) and (c).

Table 3.2: T_1 values of gel phantoms estimated using M2D FSPGR pulse sequence. The T_1 values were the average of four volunteer.

Phantom	T_1 values (ms)
A	643 ± 6
B	833 ± 17
C	926 ± 17
D	1441 ± 17
E	1769 ± 14
F	1389 ± 54
G	1637 ± 87

3.1.3 Three Dimensional Fast Spoiled Gradient Echo (3D FSPGR)

Figure 3.4(a) to (c) shows images of the gel phantoms produced by using 3D FSPGR pulse sequence with three different flip angles. Figure 3.4(d) shows the image of T_1 map produced from figure 3.4(a), (b) and (c). The colour scale beside the phantoms represents the value of T_1 map on the phantom image. The T_1 values estimated from the figure 3.4 (d) are given in table 3.3.



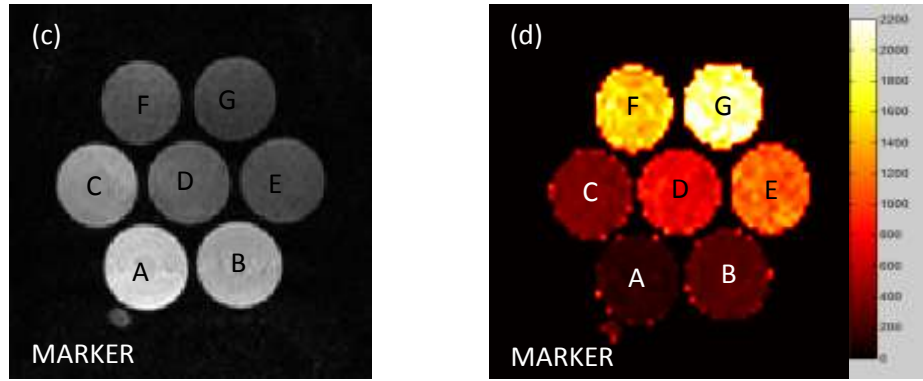


Figure 3.4: Images of gel phantoms produced using 3D FSPGR pulse sequence (TR: 11.61 ms; TE: 5.26 ms) with flip angle of: (a) 5° (b) 10° (c) 14°. (d) The T_1 map produced using images of (a), (b) and (c).

Table 3.3: T_1 values of gel phantoms using 3D FSPGR pulse sequence. The T_1 values were the average of four volunteer.

PHANTOM	T_1 value (ms)
A	135 ± 7
B	288 ± 5
C	395 ± 11
D	747 ± 1
E	1086 ± 25
F	1470 ± 14
G	2000 ± 48

3.1.4 Liver Acquisition with Volume Acceleration (3D LAVA)

Figure 3.5(a) to (c) shows images of phantoms produced by using 3D LAVA pulse sequence with three different flip angles. Figure 3.5(d) shows the image of T_1 map produced from figure 3.5(a), (b) and (c). The colour scale beside the phantoms represents the value of T_1 map on the phantom image. The value of T_1 estimated for each phantom for 3D LAVA pulse sequence obtained were given in the table 3.4.

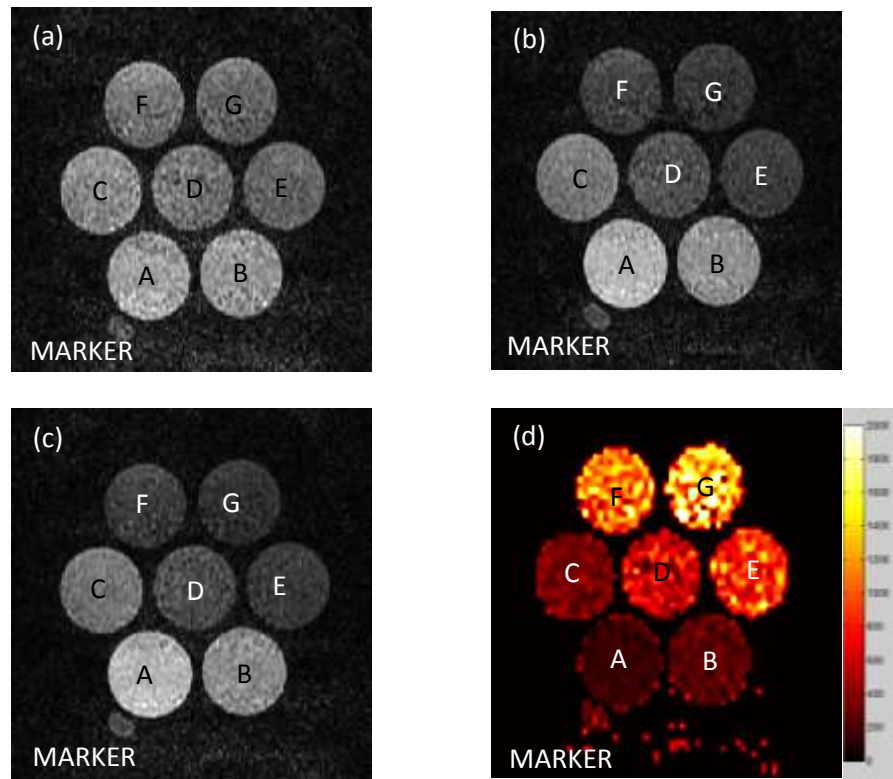


Figure 3.5: Phantoms images of 3D LAVA pulse sequence (TR: 5.27 ms; TE: 2.62 ms) with flip angle of: (a) 5° (b) 10° (c) 14°. (d) Image of phantom with T_1 map produced using images of (a), (b) and (c).

Table 3.4: T_1 values of gel phantoms using 3D LAVA pulse sequence. The T_1 values were the average of four volunteer.

Phantom	T_1 value (ms)
A	162 ± 4
B	263 ± 4
C	353 ± 19
D	601 ± 58
E	872 ± 12
F	1049 ± 30
G	1499 ± 107

3.2 Data Analysis for Phantom Imaging

3.2.1 Comparison of T_1 values of M2D FSPGR, 3D FSPGR and 3D LAVA with FSE-IR

Figure 3.6 shows the T_1 values of gel phantoms (A, B, C, D, E, F, G) using different pulse sequences; FSE-IR, M2D FSPGR, 3D FSPGR and 3D LAVA.

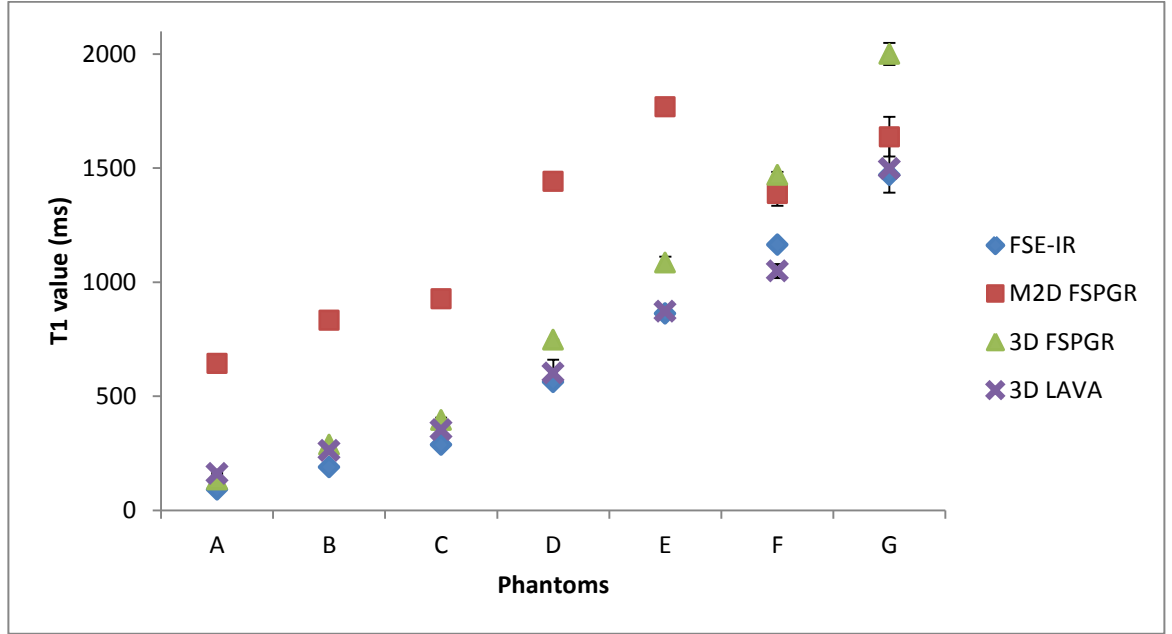


Figure 3.6: The T_1 values of gel phantom plot for different pulse sequence.

Figure 3.7 shows the percentage difference of T_1 values of gel phantom using M2D FSPGR, 3D FSPGR and 3D LAVA pulse sequences with respect to FSE-IR pulse sequence. The differences are calculated using Eq. [3.1]:

$$\frac{T_{1(pulse\ sequence)} - T_{1(FSE-IR)}}{T_{1(FSE-IR)}} \times 100\% \quad [3.1]$$

Where $T_{1(pulse\ sequence)}$ represents the value of T_1 estimated by using different VFA techniques, $T_{1(FSE-IR)}$ represents the value of T_1 at FSE-IR pulse sequence.

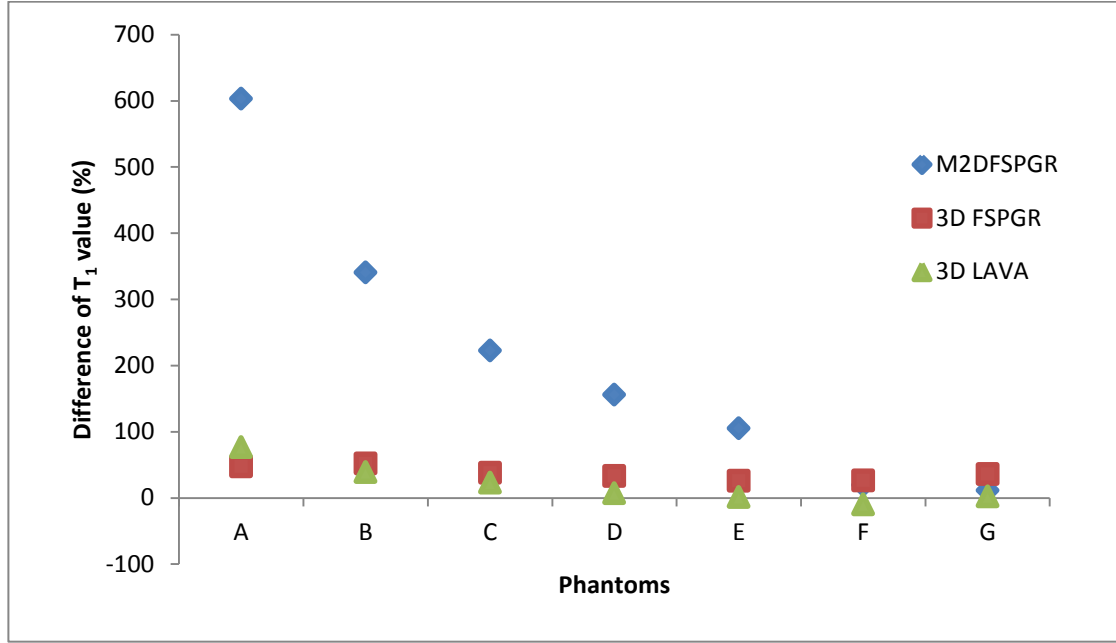


Figure 3.7: Percentage difference of T_1 values at M2D FSPGR, 3D FSPGR and 3D LAVA with respect to FSE-IR pulse sequence.

Figure 3.7 shows that the difference of T_1 values from 3D LAVA pulse sequence with FSE-IR is in the range of 1 to 77 %. For 3D FSPGR pulse sequence, the difference of T_1 values is in range 26 to 52%. While for the 2D FSPGR, the difference of T_1 value compare to FSE-IR pulse sequence which is around 11 to 603% of difference. A summary of the difference of T_1 values respect to FSE-IR (in percentage) given in table 3.5.

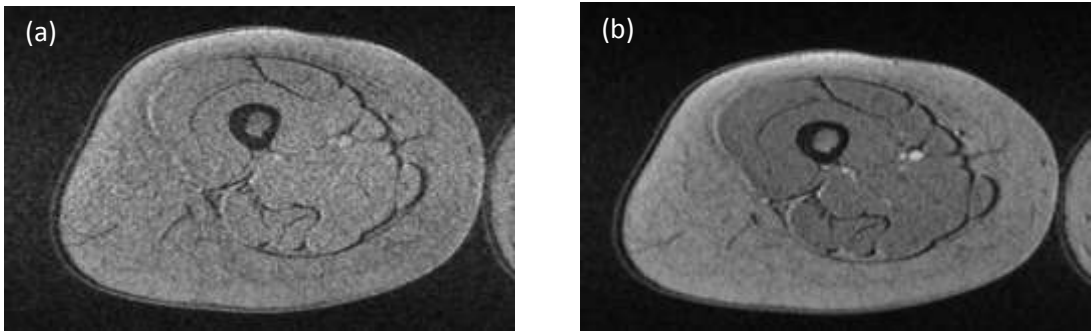
Table 3.5: The percentage difference of T_1 values respect to FSE-IR pulse sequence.

PHANTOM	Percentage Difference to FSE-IR (%)		
	M2D FSPGR	3D FSPGR	3D LAVA
A	603	47	77
B	341	52	39
C	223	38	23
D	156	33	7
E	105	29	1
F	19	26	-10
G	11	36	2

3.3 Imaging Experiment on Volunteers

3.3.1 M2D FSPGR

Figure 3.8 (a) to (c) shows an image of the right thigh of one of the volunteers acquired in axial orientation using M2D FSPGR pulse sequence with three different flip angles (5° , 10° and 14°). These three images were obtained from the same volunteer and from the same slice position. Hence, the same position of thigh is assumed. Figures 3.8 (a), (b) and (c) are the images acquired by using different flip angles, and 3.8 (d) is the T_1 map produced. The colour scale beside the image represents the T_1 values estimated.



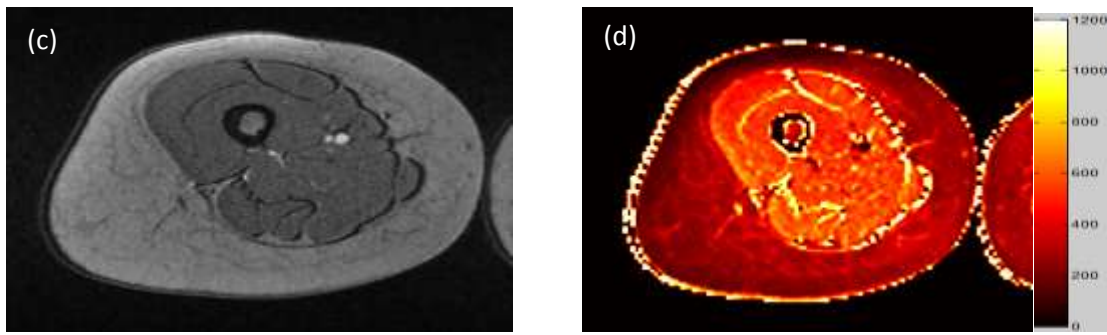
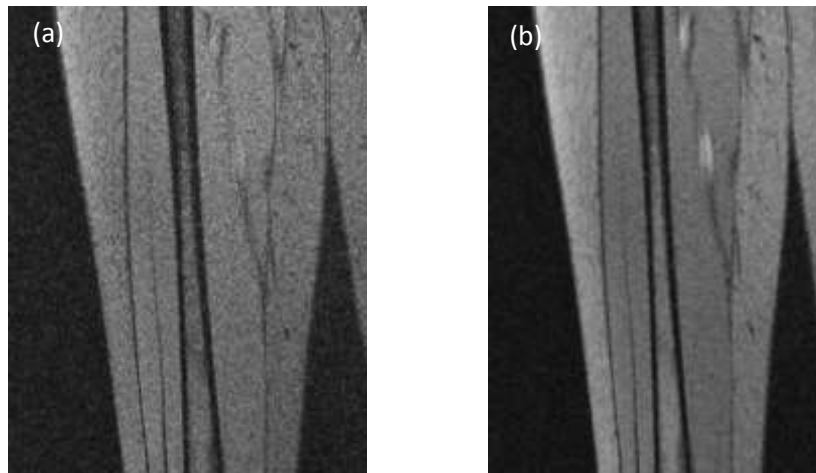


Figure 3.8: Typical images of volunteer right thigh using M2D FSPGR pulse sequence (TR: 9.1 ms; TE: 1.76 ms) at axial orientation with flip angle of (a) 5° (b) 10° (c) 14° . (d) Typical image of volunteer right thigh with T_1 map acquired from the three images (a), (b) and (c).

Figure 3.9 shows the images from the coronal orientation of scanning. The T_1 value of fat and muscles estimated from the volunteers' right thigh at axial and coronal orientation are given in table 3.6.



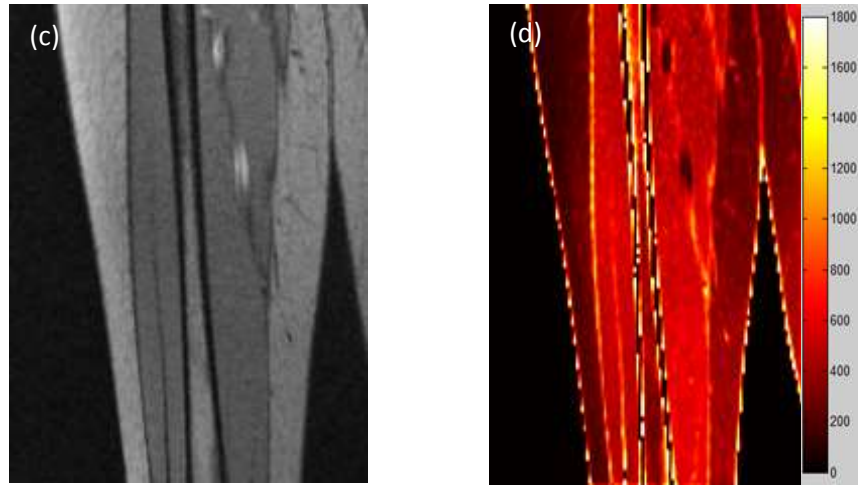


Figure 3.9: Typical images of volunteer right thigh using M2D FSPGR pulse sequence (TR: 9.1 ms; TE: 1.77 ms) at coronal orientation with flip angle of: (a) 5° (b) 10° (c) 14° . (d) Typical image of volunteer right thigh with T_1 map acquired from the three images (a), (b) and (c).

Table 3.6: T_1 values of fat and muscle by using M2D FSPGR pulse sequence at axial and coronal orientation.

Area	T_1 value (ms)	
	Axial Orientation	Coronal Orientation
Fat	217 ± 31	202 ± 32
Muscle	554 ± 32	505 ± 36

3.3.2 3D FSPGR

Figure 3.10(a) to (c) shows one of volunteer images produced by using 3D FSPGR pulse sequence with three different flip angles (5° , 10° and 14°) at axial orientation. Figure 3.10 (d) shows the T_1 map of phantom produced by using the three images with different flip angles [(a) to (c)].

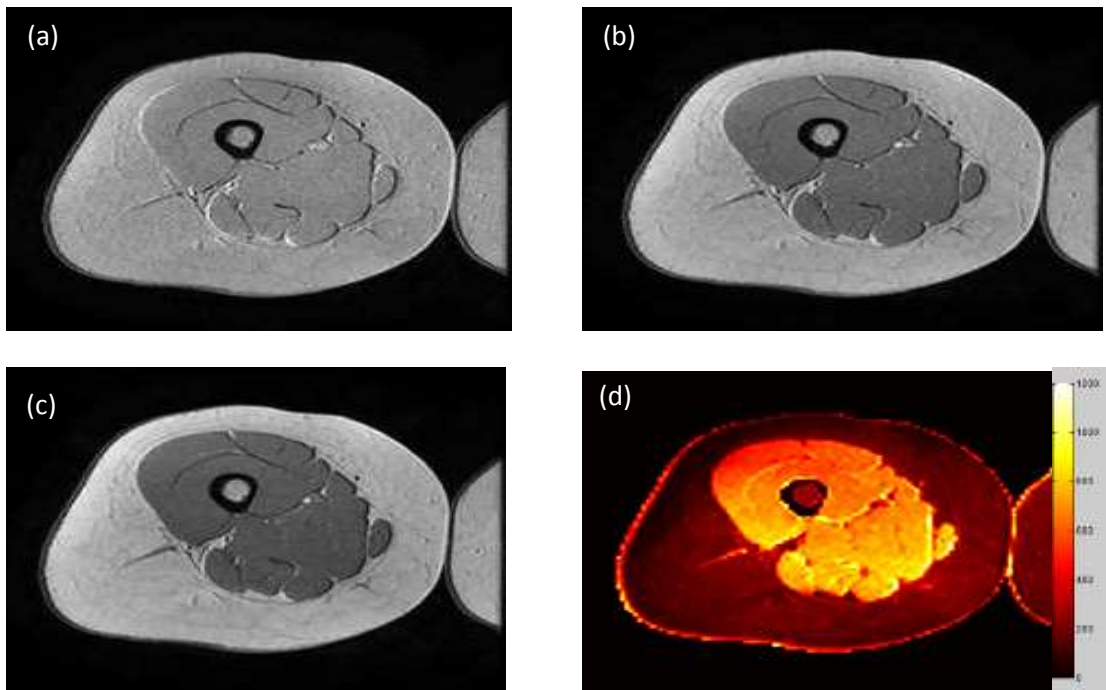
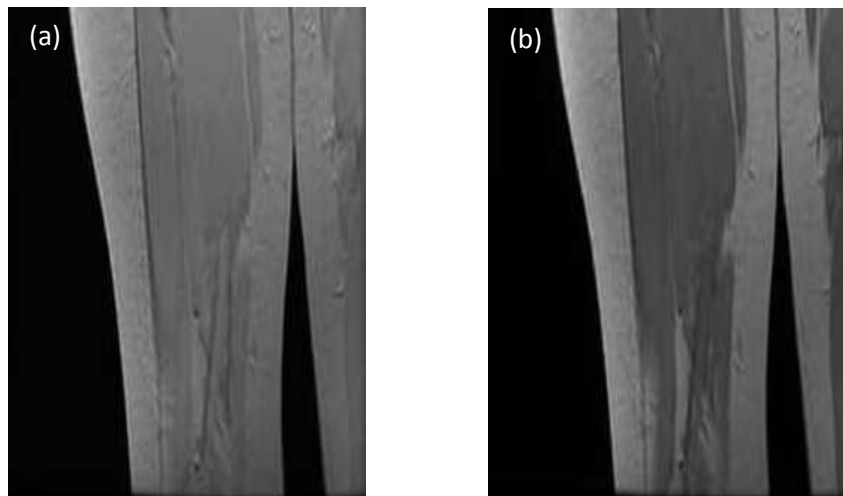


Figure 3.10: Typical images of volunteer right thigh scanned by using 3D FSPGR pulse sequence (TR: 11.52 ms; TE: 5.18 ms) at axial orientation with flip angles of (a) 5° (b) 10° (c) 14°. (d) Typical image of volunteer right thigh with T₁ map acquired from the three images (a), (b) and (c).

Figure 3.11 shows the images by using the same pulse sequence but at coronal orientation. The table 3.7 shows the T₁ value estimated for fat and muscles from volunteers' right thigh at axial and coronal orientation for 3D FSPGR pulse sequence.



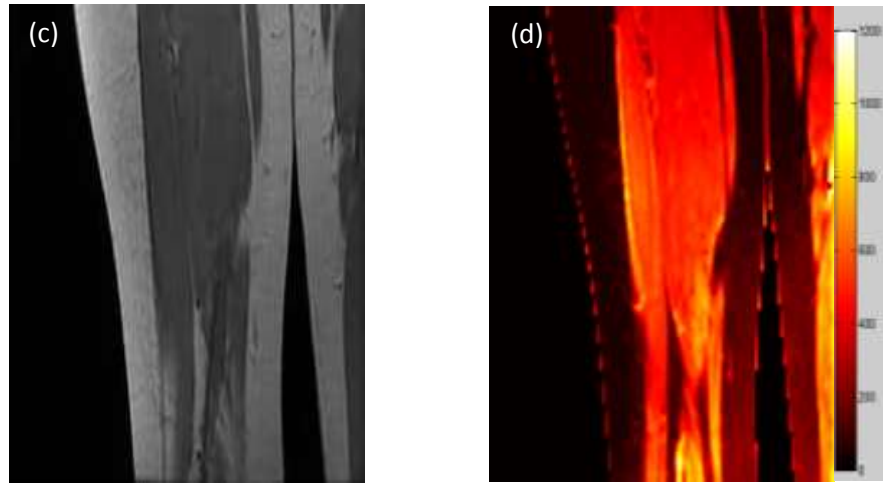


Figure 3.11: Typical images of volunteer's right thigh using 3D FSPGR pulse sequence (TR: 11.43 ms; TE: 5.1 ms) at coronal orientation with flip angle of (a) 5° (b) 10° and (c) 14° . (d) Typical image of volunteer right thigh with T_1 map acquired from the three images (a), (b) and (c).

Table 3.7: T_1 values of fat and muscle by using 3D FSPGR pulse sequence at axial and coronal orientation

Area	T_1 value (ms)	
	Axial orientation	Coronal orientation
Fat	134 ± 29	78 ± 18
Muscle	618 ± 97	397 ± 59

3.2.3 3D LAVA

Figure 3.12(a) to (c) shows one of volunteer images formed by using 3D LAVA pulse sequence with three different flip angles (5° , 10° and 14°) at axial orientation. The T_1 map image of phantom with the colour scale had illustrated on figure 3.12 (d). Each colour on the scale represents the value estimated on the phantom.

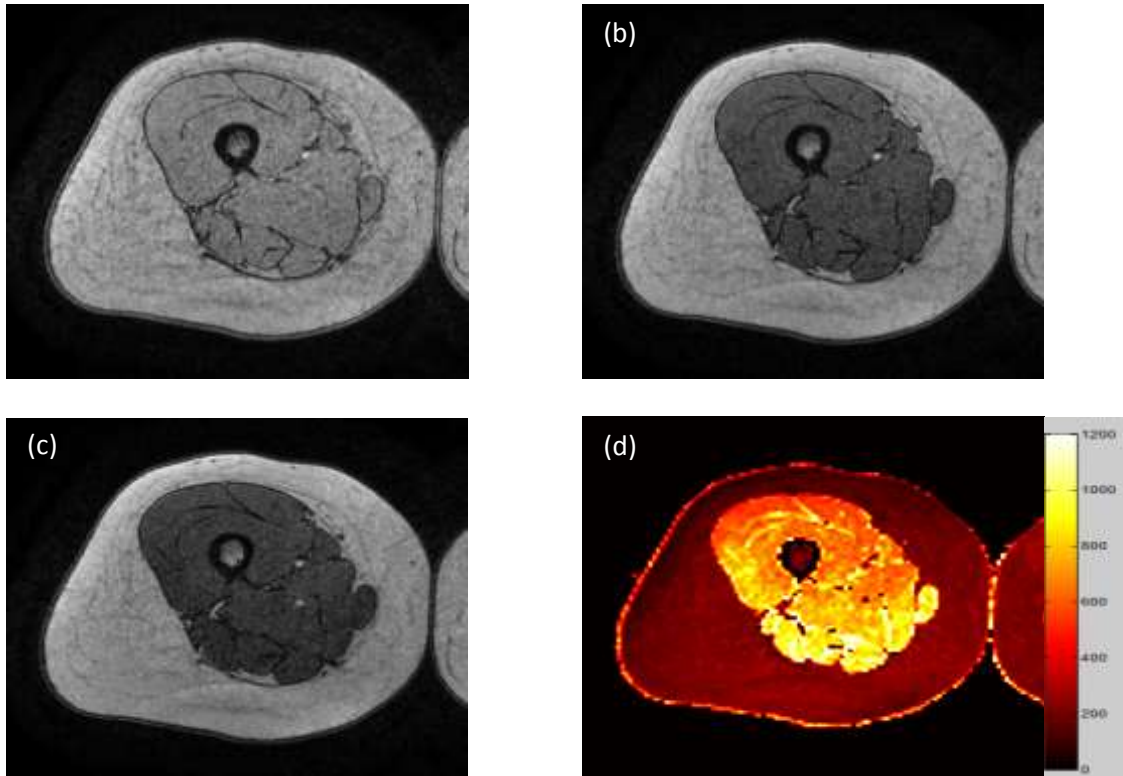


Figure 3.12: Typical images of volunteer right thigh using 3D LAVA pulse sequence (TR: 4.91 ms; TE: 2.47 ms) at axial orientation with flip angle of (a) 5° (b) 10° (c) 14° . (d) Typical Image of volunteer right thigh with T_1 map acquired from the three images (a), (b) and (c).

Figure 3.13 represents the image of phantom from similar pulse sequence but different scanning orientation. Table 3.8 shows the T_1 value estimated for fat and muscles at thigh of the volunteers using 3D LAVA pulse sequence for both orientation: axial and coronal.

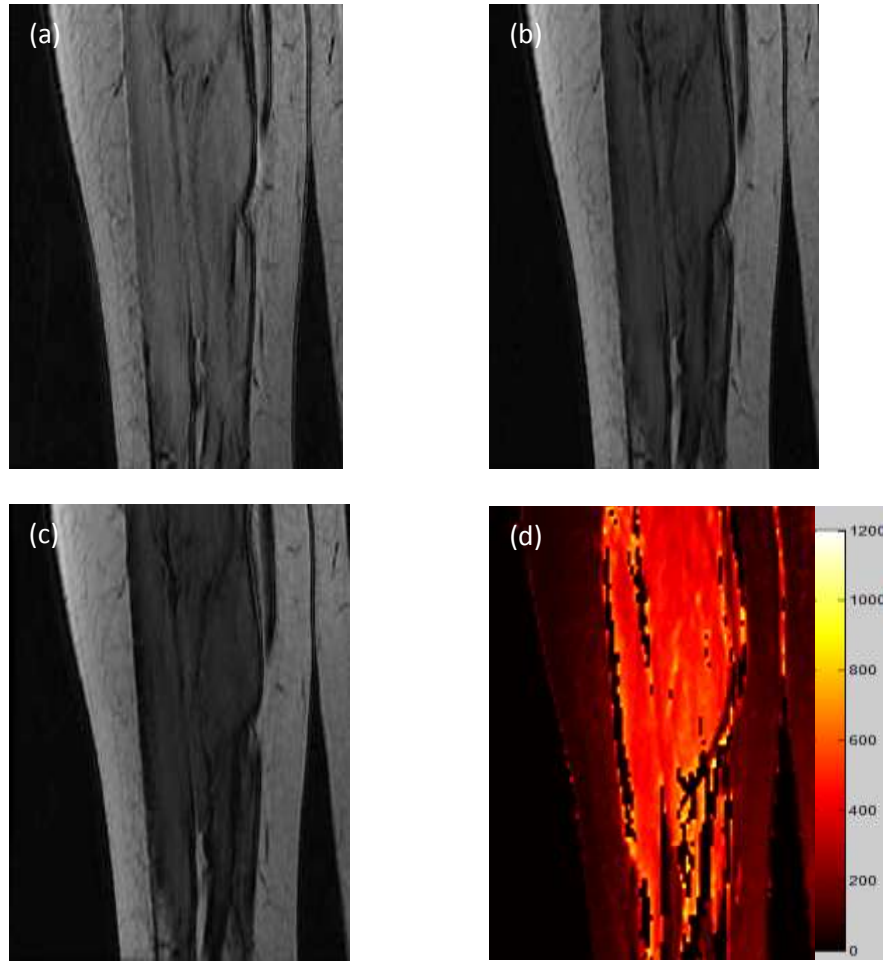


Figure 3.13: Typical images of volunteer right thigh using 3D LAVA pulse sequence (TR: 4.14 ms; TE: 2.03 ms) at coronal orientation with flip angle of (a) 5° (b) 10° (c) 14°. (d) Typical image of volunteer's right thigh with T_1 map acquired from images (a), (b) and (c).

Table 3.8: T_1 values of fat and muscle by using 3D LAVA pulse sequence at axial and coronal orientation

Area	T_1 value (ms)	
	Axial orientation	Coronal orientation
Fat	179 ± 19	95 ± 17
Muscle	637 ± 75	442 ± 22

3.4 Data Analysis for Volunteers Imaging

3.4.1 Comparison of T_1 values estimated from different anatomical orientation

Figure 3.13 and 3.14 shows the difference of T_1 values of fat and muscle of thigh measured at different anatomical orientation for three different pulse sequences.

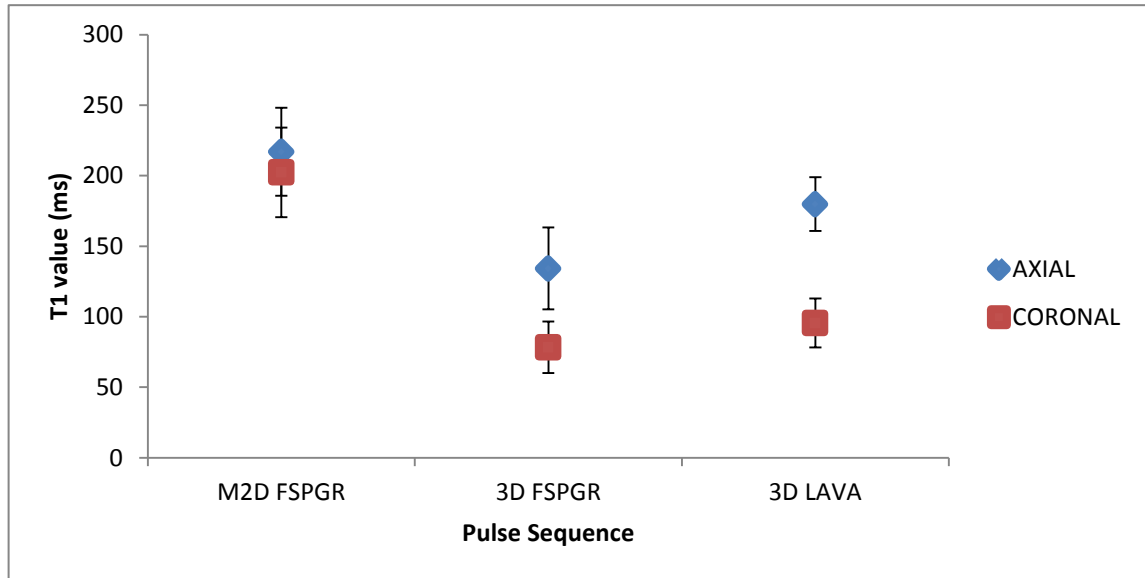


Figure 3.14: The T_1 values of fat with difference in anatomical orientation for three pulse sequences.

The T_1 value of fat shows slightly small difference between the scanning orientations which for M2D FSPGR is about 7%. While for 3D FSPGR is 42% and 3D LAVA is 47% shown large difference of T_1 value for two different scanning orientations. Figure 3.14 shows the T_1 value of fat using M2D FSPGR is higher than T_1 value estimated using 3D FSPGR and 3D LAVA for both axial and coronal scanning orientations.

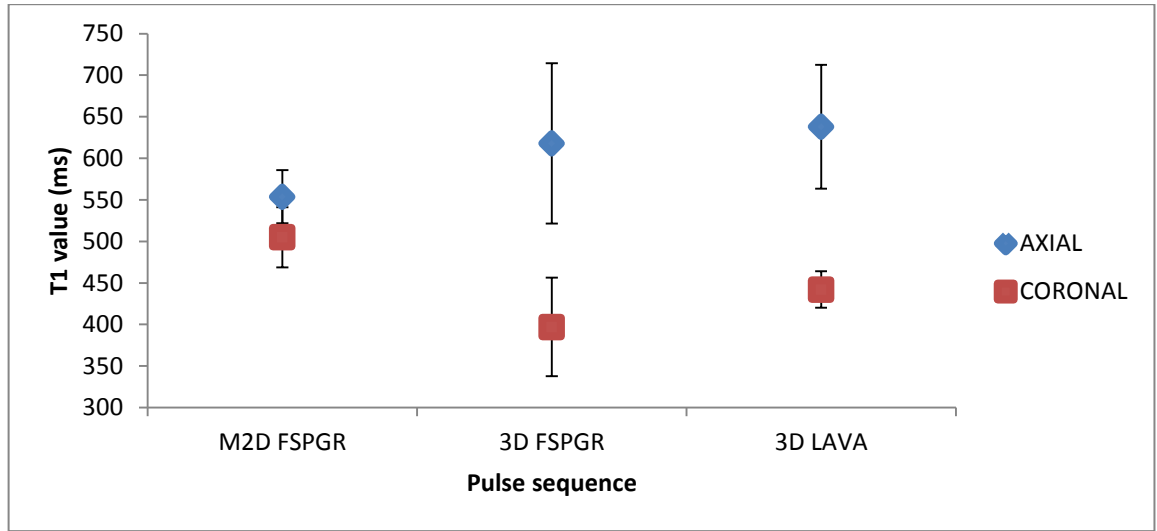


Figure 3.15: The T_1 values of muscle different with difference in anatomical orientation for three pulse sequences.

The difference of T_1 value for muscle using M2D FSPGR pulse sequence shows a smaller difference compared to 3D FSPGR and 3D LAVA for two scanning orientation which is around 9% difference, while for 3D FSPGR is 36% and 3D LAVA is 31%. Figure 3.15 shows the value of T_1 for muscle using M2D FSPGR is the highest followed by 3D LAVA and 3D FSPGR at coronal orientation. For axial orientation, the value of T_1 using M2D FSPGR is the lowest followed by 3D FSPGR and 3D LAVA.

Table 3.9 shows the difference of T_1 values of fat and muscle measured by using different scanning orientation using M2D FSPGR, 3D FSPGR and 3D LAVA pulse sequences. The percentage differences are calculated using Eq. [3.2].

$$\frac{T_{1(coronal)} - T_{1(axial)}}{T_{1(coronal)}} \times 100 \quad [3.2]$$

where $T_{1(\text{coronal})}$ represents the value of T_1 at coronal orientation, $T_{1(\text{axial})}$ represents the value of T_1 at axial orientation. Both T_1 values were measured from the same pulse sequence.

Table 3.9: The percentage difference of T_1 values for different scanning orientation using three pulse sequences

	M2D FSPGR			3D FSPGR			3D LAVA		
	T_1 value (ms)		% Diff	T_1 value (ms)		% Diff	T_1 value (ms)		% Diff
	AX	COR		AX	COR		AX	COR	
Fat	217	202	-7	134	78	-42	180	95	-47
Muscle	554	505	-9	618	397	-36	638	442	-31

3.4.2 Comparison of T_1 values estimated for different scanning technique

Figure 3.16 and 3.17 show comparison of T_1 values obtained using M2D and 3D FSPGR pulse sequence at fat and muscle of thigh.

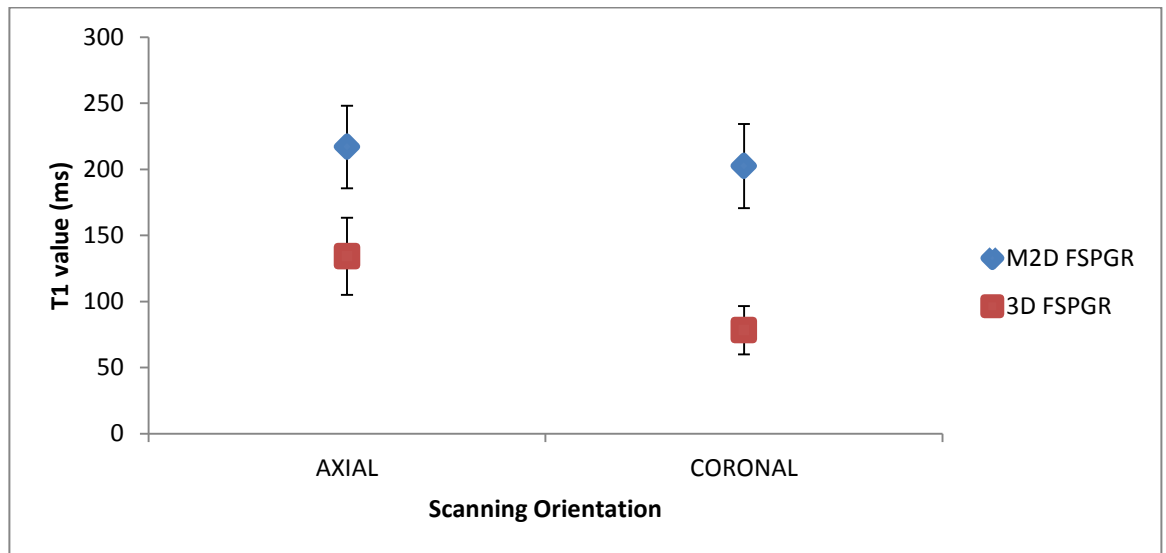


Figure 3.16: The T_1 values of fat with different in scanning technique for FSPGR pulse sequence.

Figure 3.16 shows the difference between dimensional scanning techniques i.e. M2D FSPGR and 3D FSPGR at axial orientation for fat has smaller difference compared to the difference of T_1 at coronal orientation about 62% and 159% respectively. The T_1 value estimated using M2D FSPGR is higher than T_1 value using 3D FSPGR for both scanning orientations.

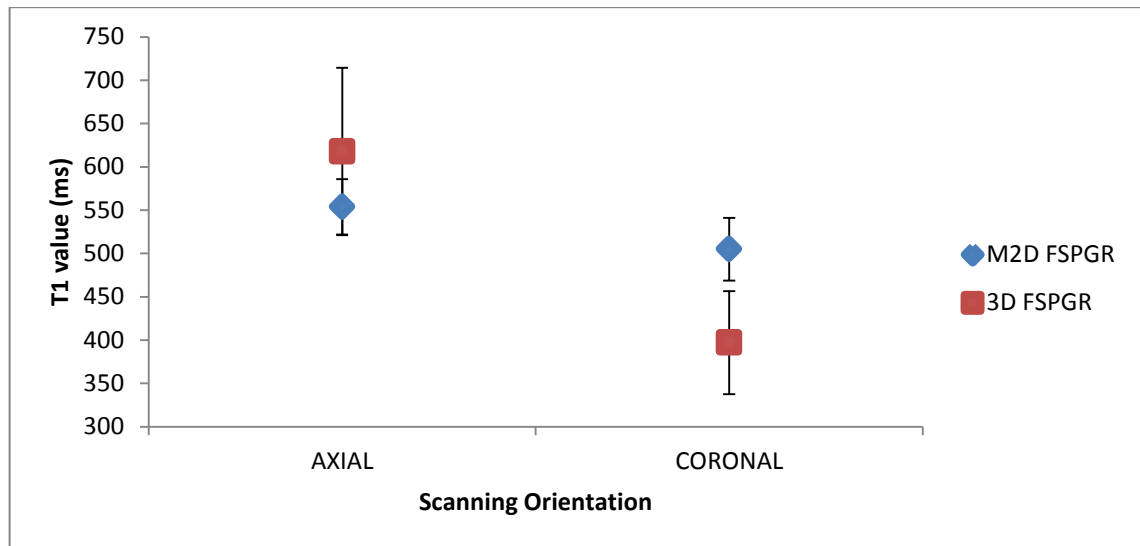


Figure 3.17: The T_1 values of muscle different with difference in scanning technique for FSPGR pulse sequence.

Figure 3.17 shows the difference of T_1 value between dimensional scanning techniques at axial orientation for muscle is smaller than difference at coronal orientation about 10% and 27% respectively. At axial orientation, the value of T_1 estimated is higher using 3D FSPGR compared with the value of T_1 using M2D FSPGR. While at coronal orientation, the T_1 value shows the opposite result using M2D FSPGR is higher than 3D FSPGR pulse sequence.

Table 3.10 shows the percentage difference of T_1 values of fat and muscle using M2D FSPGR pulse sequence with respect to 3D FSPGR pulse sequence. The percentage differences were calculated using Eq. [3.3].

$$\frac{T_{1(2D\ FSPGR)} - T_{1(3D\ FSPGR)}}{T_{1(3D\ FSPGR)}} \times 100 \quad [3.3]$$

where $T_{1(2D\ FSPGR)}$ represents the value of T_1 by using M2D FSPGR pulse sequence, $T_{1(3D\ FSPGR)}$ represents the value of T_1 by using 3D FSPGR pulse sequence. Both T_1 values are from the same scanning orientation; axial orientation or coronal orientation.

Table 3.10: The percentage difference of T_1 values for difference dimensional of scanning technique with respect to 3D FSPGR

	AXIAL			CORONAL		
	T_1 value (ms)		% Difference	T_1 value (ms)		% Difference
	M2D FSPGR	3D FSPGR		M2D FSPGR	3D FSPGR	
Fat	217	134	62	202	78	159
Muscle	554	618	-10	505	397	27

3.4.3 Comparison of T_1 values estimated using different pulse sequence

Figures 3.18 and 3.19 show the difference of T_1 values using different pulse sequences at two anatomical orientations for fat and muscle of thigh.

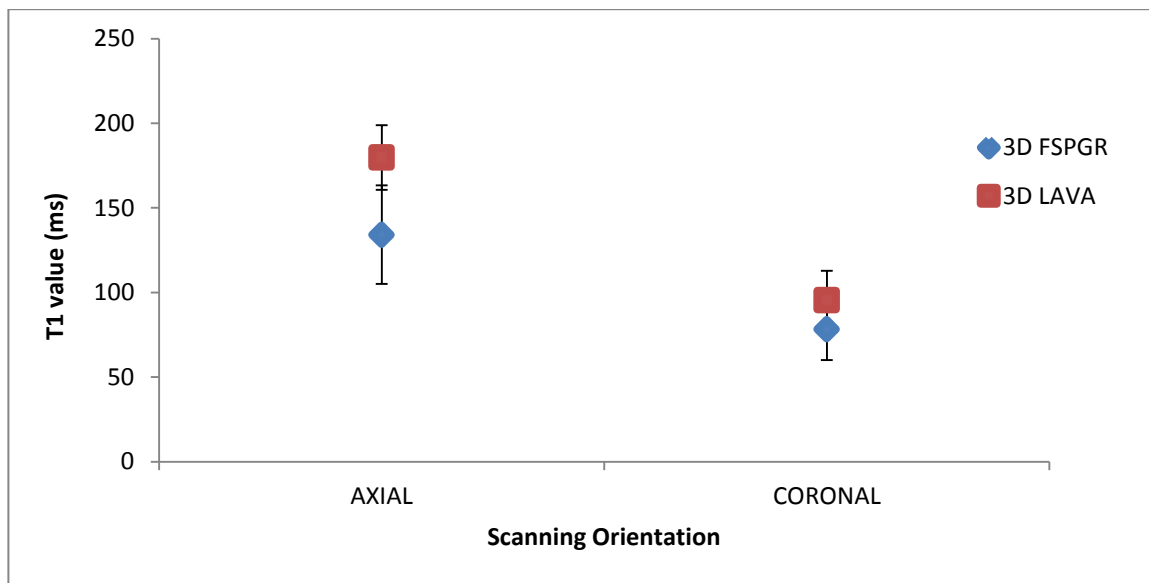


Figure 3.18: The T_1 values of fat with difference pulse sequence for two orientations.

The difference of T_1 value of fat using 3D LAVA and 3D FSPGR is small at coronal orientation compared with the T_1 value at axial orientation. The difference is about 34% at axial orientation and 21.9% at coronal orientation. The T_1 value of fat using 3D LAVA is slightly higher than 3D FSPGR for both orientations.

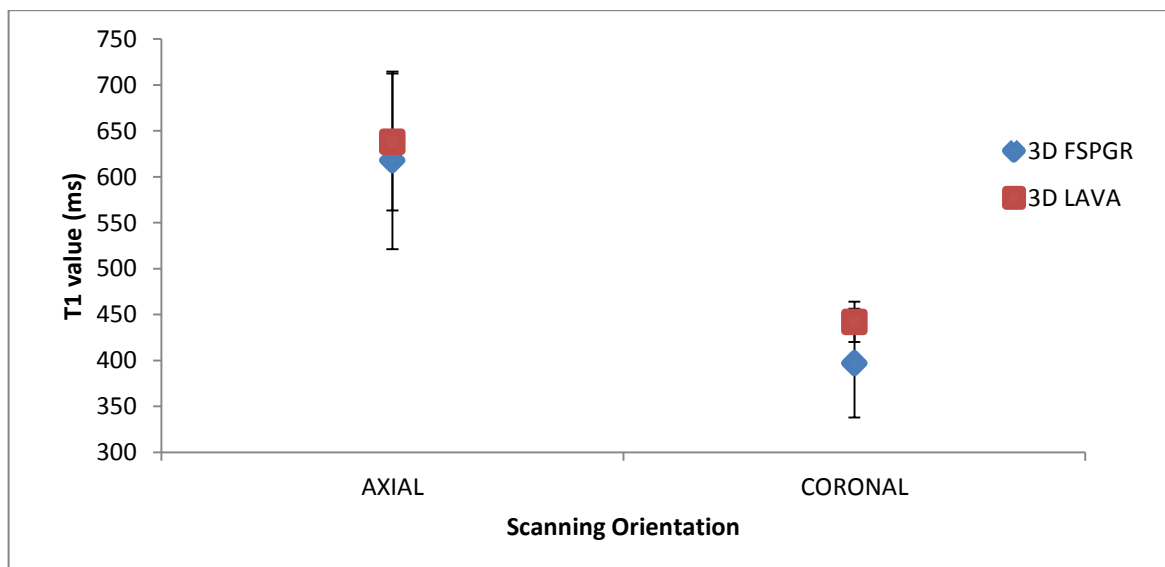


Figure 3.19: The T_1 values of muscle different with difference pulse sequence for two orientations.

The difference of T_1 value of muscle using 3D LAVA and 3D FSPGR is small at axial orientation compare with the T_1 value at coronal orientation. The difference is about 3% at axial orientation and 11% at coronal orientation. The T_1 value of muscle using 3D LAVA is slightly higher than 3D FSPGR for both orientations.

Table 3.11 shows the percentage difference of T_1 values of fat and muscle using 3D LAVA pulse sequences with respect to 3D FSPGR pulse sequence. The percentage differences are calculated using Eq. [3.4]:

$$\frac{T_{1(LAVA)} - T_{1(3D\ FSPGR)}}{T_{1(3D\ FSPGR)}} \times 100 \quad [3.4]$$

Where $T_{1(LAVA)}$ represents the value of T_1 by using 3D LAVA pulse sequence, $T_{1(3D\ FSPGR)}$ represents the value of T_1 by using 3D FSPGR pulse sequence. Both T_1 values are from the same scanning orientation i.e., axial or coronal orientation.

Table 3.11: The percentage difference of T_1 values for 3D LAVA with respect to 3D FSPGR pulse sequence

	AXIAL			CORONAL		
	T_1 value (ms)		% Difference	T_1 value (ms)		% Difference
	3D LAVA	3D FSPGR		3D LAVA	3D FSPGR	
Fat	180	134	34	95	78	22
Muscle	638	618	3	442	397	11

CHAPTER 4

DISCUSSION

4.1 Imaging Experiment on Gel Phantom

4.1.1 Fast Spin Echo Inversion Recovery (FSE-IR)

Inversion recovery pulse sequence is considered as the standard technique to measure T_1 (Steen et al., 1994). By using this technique the imaging is repeated several times each one with different TI. Ideally, the TR should be at least five times the maximum T_1 values of the subject. The maximum T_1 value in the phantom study was 1470 ms and the TR is 6500 ms. The TR value used in this study approximately five times the maximum of the T_1 value i.e., 4.4 times of maximum T_1 . A long imaging time is required to measure T_1 by using this technique because of the long TR used. Longer acquisition time is required if a longer TR is used. Hence, this technique is not normally used to measure T_1 in patients or volunteers especially by using 3D acquisition technique.

4.1.2 Comparison of T_1 values of M2D FSPGR, 3D FSPGR and 3D LAVA with IR-FSE

Figure 3.6 shows the pattern of the T_1 values for each phantom acquired by using FSE-IR, 3D FSPGR and 3D LAVA. The T_1 value increases from phantom A to G. Note

that the concentration of the gel phantom is the highest in phantom A and the lowest in phantom G (see table 2.1). However, for the M2D FSPGR, the T_1 value only increases for the first five phantoms (A to E) and the T_1 values of phantom F and G are lower than phantom E.

In this experiment, it was found that the T_1 values measured in the gel phantoms are dependent on the imaging technique used. Figure 3.7 shows the difference of T_1 values (in percentage) for three techniques i.e. M2D FSPGR, 3D FSPGR and 3D LAVA relative to FSE-IR pulse sequence. It was found that the values of T_1 measured by using 3D LAVA and 3D FSPGR are very similar to the FSE-IR which is considered as the standard T_1 measurement technique. The M2D FSPGR pulse sequence shows a much higher difference compared to other pulse sequences especially for the phantoms with short T_1 values (Phantom A-E). However, for the phantoms with long T_1 (F and G), the values are very close to the values obtained using FSE-IR.

The high differences of the T_1 values measured between the M2D FSPGR and FSE-IR may be due to the crosstalk between the slices in the M2D technique. The individual slice profile for each individual slice acquired by using the 2D acquisition technique is nonrectangular (Hänicke et al., 1988). Part of the slices may overlap with each other if the slice gaps are very close. Hence, it may affect the signal intensities and the T_1 values measured on the gel phantoms.

The 3D LAVA pulse sequence is basically based on 3D FSPGR sequence ("LAVA sequence MRI," 2013). Therefore, the value of T_1 produced from both 3D LAVA and 3D FSPGR should be very close to each other if the same parameters are used.

4.2 Imaging Experiment on Volunteers

4.2.1 Comparison of T_1 values estimated from different anatomical orientation

In this study, it was found that the T_1 values in fat and muscle of the thigh varied with the scanning orientation applied in the MRI procedure. Figures 3.13 and 3.14 show that the value of T_1 at fat and muscle of volunteers at axial orientation is measure as higher than at coronal scanning orientation for all three different pulse sequences i.e M2D FSPGR, 3D FSPGR and 3D LAVA. This difference may be due to the influence of blood flow in the tissue.

The slightly lower values of all T_1 values of muscle and fat compared to the literature values may be due to the different anatomical regions of the tissue, for example abdominal fat may be have different molecular composition compared to breast fat. Hence the tissues might have different T_1 values. It is the same for muscle, the T_1 value of muscle in the abdomen may be not be the same as the value at lower extremities. Another possible explanation is the T_1 may be affected by the factors such as gender, age, ethnicity, and their lifestyle.

4.2.2 Comparison of T_1 values estimated from different scanning dimensional

In this study, we noticed that the T_1 values in fat and muscle of thigh varied with the dimensional of all scanning technique applied during MRI procedure. Figures 3.16 and 3.17 demonstrate that the value of T_1 at fat and muscle of volunteers for M2D FSPGR and 3D

FSPGR at axial and coronal. The value of T_1 of fat shows large differences between two differences dimensional scanning while skeletal muscle shows slightly smaller difference.

4.2.3 Comparison of T_1 values of difference pulse sequence

In this study, we noticed the T_1 values in fat and muscle of thigh varied with the pulse sequence applied during the MRI procedure. Figures 3.18 and 3.19 demonstrate that the value of T_1 of fat and muscle of volunteers for 3D FSPGR and 3D LAVA. The difference of T_1 value of fat at axial and coronal orientation has small difference compare with the T_1 value of muscle. The difference is 34% and 21.9% at for fat and 3.3% and 11.3% for muscle respectively.

The T_1 value for muscle using 3D FSPGR and 3D LAVA pulse sequences shows very similar values. Basically, the 3D LAVA pulse sequence protocol is based on the 3D FSPGR. In its standard form the 3D LAVA pulse sequence employs fat saturation. However in this study, the function was disabled. Small differences in the T_1 values measured by using 3D LAVA and 3D FSPGR may be due to the different parameter setting used in both pulse sequences such the TR and TE.

CHAPTER 5

CONCLUSIONS

5.1 Conclusion

DCE-MRI is considered as one of the most sensitive imaging technique to detect cancer. In clinical setting, a qualitative technique normally based on visual inspection of signal enhancement curves is used in the diagnosis. However this technique is dependent on the scanning technique used. Hence, quantitative techniques that can produce pharmacokinetic parameters such as k^{trans} and v_e have been introduced (Tofts, 1997). Normally, the native T_1 values of the tissues are measured and applied in the parameters estimation. Hence, any error in the T_1 measured will influence the accuracy of the pharmacokinetic parameters estimated.

For the comparison of T_1 values measured using different pulse sequence i.e. M2D FSPGR, 3D FSPGR and 3D LAVA with FSE-IR at 1.5 Tesla, it was found that the T_1 value by 3D FSPGR and 3D LAVA were closest to value to the T_1 value measured by the standard T_1 measurement technique i.e. FSE-IR. However the T_1 values measured using M2D FSPGR pulse sequence showed a substantial difference compared to the T_1 values measured by FSE-IR.

From experiments on phantom it was found that the T_1 value measured by using 3D image acquisition is much closer to the IR method compared to M2D imaging. The reduction in the accuracy of T_1 especially at short T_1 may be due to the crosstalk between the slices. Hence, it can be assumed that both the 3D FSPGR and LAVA are the techniques that should be used to measure T_1 values in phantoms, while the M2D FSPGR technique should not be used for this purpose.

The T_1 values also are affected by the scanning orientation used in the experiment. From the experiments performed, the axial orientation give the higher T_1 value compared to coronal orientation for all the three pulse sequences, M2D FSPGR, 3D FSPGR and 3D LAVA. This may be due to the effect of blood flow in the tissue, the signal intensity and image contrast, which than affected the T_1 values estimated.

Variable flip angle (VFA) using 3D FSPGR and 3D LAVA pulse sequences produce very similar T_1 values. This may be due to 3D LAVA is a modified version of 3D FSPGR pulse sequences. Note that 3D LAVA has a special parallel imaging technique to reduce the scanning time.

5.2 Limitation of this study

Due to the time constrain and the scanner's busy schedule, only four volunteers were able to be scanned for this study. This may affect the accuracy of the results.

The T_1 values of the fat and muscle reported in the literature are from different anatomical locations of the volunteers and were measured in western countries. Hence, the T_1 values measured in this experiment cannot be directly compared with the values reported.

5.3 Future works

The experiments on volunteers of this study only involve four volunteers. Hence, to increase the validity of the results should be planned to include more volunteers for this purpose in the future (up to 10 volunteers as approved by the ethic committee). It is also proposed that the experiment can also be performed by using 3 Tesla MRI.

REFERENCE

- Allison, Jerry, & Yanasak, Nathan. (2010). Basic MRI Method
- Brookes, Jason A., Redpath, Thomas W., Gilbert, Fiona J., Murray, Alison D., & Staff, Roger T. (1999). Accuracy of T1 measurement in dynamic contrast-enhanced breast MRI using two- and three-dimensional variable flip angle fast low-angle shot. *Journal of Magnetic Resonance Imaging*, 9(2), 163-171. doi: 10.1002/(SICI)1522-2586(199902)9:2<163::AID-JMRI3>3.0.CO;2-L
- Buckley, David L, & Parker, Geoffrey J M. (2005). Measuring Contrast Agent Concentration in T1-Weighted Dynamic Contrast-Enhanced MRI. In A. Jackson, D. Buckley & G. M. Parker (Eds.), *Dynamic Contrast-Enhanced Magnetic Resonance Imaging in Oncology* (pp. 69-79): Springer Berlin Heidelberg.
- Bushberg, J.T., Seibert, J.A., Leidholdt, E.M., & Boone, J.M. (2002). *The Essential Physics of Medical Imaging*: Wolters Kluwer Health.
- de Bazelaire, Cedric MJ, Duhamel, Guillaume D, Rofsky, Neil M, & Alsop, David C. (2004). MR imaging relaxation times of abdominal and pelvic tissues measured in vivo at 3.0 T: preliminary results1. *Radiology*, 230(3), 652-659.
- Dhawan, Atam P. (2011). *Medical Image Analysis* (2 ed.). New Jersey: John Wiley & Sons, Inc
- Han, E, Gold, G, Stainsby, J, Wright, G, Beaulieu, C, & Brittain, J. (2003). *In-vivo T1 and T2 measurements of musculoskeletal tissue at 3T and 1.5 T*. Paper presented at the Proceedings of the 11th Annual Meeting of ISMRM, Toronto, Canada.
- Hänicke, Wolfgang, Merboldt, Klaus-Dietmar, & Frahm, Jens. (1988). Slice selection and T1 contrast in FLASH NMR imaging. *Journal of Magnetic Resonance* (1969), 77(1), 64-74. doi: [http://dx.doi.org/10.1016/0022-2364\(88\)90032-7](http://dx.doi.org/10.1016/0022-2364(88)90032-7)
- Henderson, Elizabeth, Sykes, Jane, Drost, Dick, Weinmann, Hanns-Joachim, Rutt, Brian K, & Lee, Ting-Yim. (2000). Simultaneous MRI measurement of blood flow, blood


- volume, and capillary permeability in mammary tumors using two different contrast agents. *Journal of Magnetic Resonance Imaging*, 12(6), 991-1003.
- Higgins, Charles B, & Hricak, Hedvig. (1987). Magnetic resonance imaging of the body.
- Kirsch, John K. (1991). Basic principles of magnetic resonance contrast agents. *Topics in Magnetic Resonance Imaging*, 3(2), 1-18.
- LAVA sequence MRI. (2013). Retrieved November 2012 from Member of SoftWays' Medical Imaging Group
<http://www.mrtip.com/serv1.php?type=db1&dbs=LAVA%20SEQUENCE%20MRI>
- Lin, W, & Song, HK. (2009). *Improved accuracy in T1 mapping and flip angle correction with random spoiling in radial gradient echo imaging*. Paper presented at the Proc. Intl. Soc. Mag. Reson. Med.
- Lin, Yen Hwa. (2012). T1 Measurement Techniques in Magnetic Resonance Imaging.
- Low, Russell N., Bayram, Ersin, Panchal, Neeraj J., & Estkowski, Lloyd. (2010). High-Resolution Double Arterial Phase Hepatic MRI Using Adaptive 2D Centric View Ordering: Initial Clinical Experience. *American Journal of Roentgenology*, 194(4), 947-956. doi: 10.2214/AJR.09.2507
- McRobbie, Donald W., Moore, Elizabeth A., Graves, Martin J., & Prince, Martin R. (2007). *MRI From Picture of Proton* (2 ed.). United States of America Cambridge University Press.
- Nitz, Wolfgang R, Balzer, Thomas, Grosu, Daniel S, & Allkemper, Thomas. (2010). Principles of Magnetic Resonance *Clinical MR Imaging* (pp. 1-105): Springer.
- Steen, R Grant, Gronemeyer, Suzanne A, Kingsley, Peter B, Reddick, Wilbum E, Langston, James S, & Taylor, June S. (1994). Precise and accurate measurement of proton T1 in human brain in vivo: validation and preliminary clinical application. *Journal of Magnetic Resonance Imaging*, 4(5), 681-691.
- Rakow-Penner, Rebecca, Daniel, Bruce, Yu, Huanzhou, Sawyer-Glover, Anne, & Glover, Gary H. (2006). Relaxation times of breast tissue at 1.5T and 3T measured using IDEAL. *Journal of Magnetic Resonance Imaging*, 23(1), 87-91. doi: 10.1002/jmri.20469

- Raymond, Kenneth N, & Pierre, Valérie C. (2005). Next generation, high relaxivity gadolinium MRI agents. *Bioconjugate chemistry*, 16(1), 3-8.
- Tofts, Paul S. (1997). Modeling tracer kinetics in dynamic Gd-DTPA MR imaging. *Journal of Magnetic Resonance Imaging*, 7(1), 91-101.

APPENDIX

Appendix A

Appendix A (i): Ethic approval form from the Medical Ethics Committee

 UNIVERSITI MALAYA PUSAT PERUBATAN UM	MEDICAL ETHICS COMMITTEE UNIVERSITY MALAYA MEDICAL CENTRE ADDRESS: LEMBAH PANTAI, 59100 KUALA LUMPUR, MALAYSIA TELEPHONE: 03-79493209 / 2251 FAXIMILE: 03-79492030
---	---

NAME OF ETHICS COMMITTEE/IRB: Medical Ethics Committee, University Malaya Medical Centre ADDRESS: LEMBAH PANTAI 59100 KUALA LUMPUR	ETHICS COMMITTEE/IRB REFERENCE NUMBER: 975.29
PROTOCOL NO (if applicable): - TITLE: T, mapping for DCE-MRI	VERSION NO.: -
PRINCIPAL INVESTIGATOR: Miss Nurun Najwa Kamaluzaman	SPONSOR: -

The following item ☒ have been received and reviewed in connection with the above study to be conducted by the above investigator.

<input checked="" type="checkbox"/> Application to Conduct Research Project (form)	Ver date: 27 Feb 13
<input checked="" type="checkbox"/> Study Protocol	Ver date:
<input type="checkbox"/> Investigator Brochure	Ver date:
<input checked="" type="checkbox"/> Patient Information Sheet	Ver date:
<input type="checkbox"/> Consent Form	Ver date:
<input type="checkbox"/> Questionnaire	Ver date:
<input checked="" type="checkbox"/> Investigator's CV (Miss Nurun Najwa Kamaluzaman)	Ver date:

and the decision is ☒ :

☒ Approved
☐ Modification requested (item specified below or in accompanying letter)
☐ Rejected (reasons specified below or in accompanying letter)

Comments:

Investigator are required to:

- 1) follow instructions, guidelines and requirements of the Medical Ethics Committee.
- 2) report any protocol deviations/violations to Medical Ethics Committee.
- 3) provide annual and closure reports to the Medical Ethics Committee.
- 4) comply with International Conference on Harmonization – Guidelines for Good Clinical Practice (ICH-GCP) and the Declaration of Helsinki.
- 5) obtain permission from the Director of UMMC before starting research that involves recruitment of UMMC patients.
- 6) ensure that if the research is sponsored, the usage of consumable items and laboratory tests from UMMC services are not charged in the patient's hospital bills but are borne by the research grant.
- 7) note that he/she can appeal to the Chairman of MEC for studies that are rejected.
- 8) note that Medical Ethics Committee may audit the approved study.
- 9) ensure that the study does not take precedence over the safety of subjects.

Date of meeting: -
 Date of approval: 07th MARCH 2013

c.c Head
Department of Biomedical Imaging

Deputy Dean (Research)
Faculty of Medicine

Secretary
Medical Ethics Committee
University Malaya Medical Centre


PROF. DATUK LOOI LAI MENG
 Chairman
Medical Ethics Committee



**UNIVERSITI
MALAYA**

PUSAT PERUBATAN UM

MEDICAL ETHICS COMMITTEE

UNIVERSITY MALAYA MEDICAL CENTRE

ADDRESS: LEMBAH PANTAI, 59100 KUALA LUMPUR, MALAYSIA

TELEPHONE: 03-79493209 / 2251 FAXIMILE: 03-79492030

MEDICAL ETHICS COMMITTEE COMPOSITION, UNIVERSITY MALAYA MEDICAL CENTRE

Date: 20th MARCH 2013

Member (Title and Name)	Occupation (Designation)	Male/Female (M/F)	Tick (✓) if present when above items were reviewed
Chairperson: Y. Bhg. Prof. Datuk Looi Lai Meng	Senior Consultant (Adjunct Professor) Department of Pathology	Female	✓
Deputy Chairperson: Prof. Kulenthiran Arumugam	Senior Consultant Medical Education Research and Development Unit (MERDU)	Male	✓
Secretary (non-voting): Puan Norashikin Mahmood	Scientific Officer Department of Quality, UMMC	Female	✓
Members: 1. Y. Bhg. Prof. Dato' Patrick Tan Seow Koon	Deputy Director (Professional) University Malaya Medical Centre	Male	✓
2. Prof. Philip Poi Jun Hua	Representative of Head Department of Medicine	Male	✓
3. Puan Syireen Alwi	Representative of Head Department of Pharmacy	Female	✓
4. Assoc. Prof. Ahmad Hatim Sulaiman	Head Department of Psychological Medicine	Male	✓
5. Assoc. Prof. Ong Teng Aik	Representative of Head Department of Surgery	Male	✓
6. Tuan Haji Amrahi Buang	Head of Pharmacist Department of Pharmacy University Malaya Medical Centre	Male	✓
7. Y. Bhg. Assoc. Prof. Datin Grace Xavier	Representative of Dean (Research Fellow) Faculty of Law University Malaya	Female	✓
8. Y. Bhg. Datin Aminah bt. Pti Abdul Rahman	Public Representative	Female	✓
9. Madam Ong Eng Lee	Public Representative	Female	

Comments: The MEC of University Malaya Medical Centre is operating according to ICH-GCP guidelines and the Declaration of Helsinki. Member's no. 7, 8 & 9 are representatives from Faculty of Law in the University Malaya and the public. They are independent of the hospital or trial site.

PROF. DATUK LOOI LAI MENG

Chairman

Medical Ethics Committee

Appendix A (ii): Sample of consent form given to volunteers

UNIVERSITY MALAYA MEDICAL CENTRE

CONSENT BY VOLUNTEER FOR CLINICAL RESEARCH

I,
 Identity Card No.
 (Name of Volunteer)
 of
 (Address)
 hereby agree to take part in the clinical research (clinical study/questionnaire study/drug trial) specified below:

Title of Study: T₁ mapping for DCE-MRI
 the nature and purpose of which has been explained to me by
 Dr.
 (Name & Designation of Doctor)
 and interpreted by
 (Name & Designation of Interpreter)
 to the best of his/her ability in language/dialect.

I have been told about the nature of the clinical research in terms of methodology, possible adverse effects and complications (as per patient information sheet). After knowing and understanding all the possible advantages and disadvantages of this clinical research, I voluntarily consent of my own free will to participate in the clinical research specified above.

I understand that I can withdraw from this clinical research at any time without assigning any reason whatsoever and in such a situation shall not be denied the benefits of usual treatment by the attending doctors.

Date: Signature or Thumbprint
 (Volunteer)

IN THE PRESENCE OF

Name)
 Identity Card No.) Signature
 (Witness for Signature of Volunteer)
 Designation)

I confirm that I have explained to the patient the nature and purpose of the above-mentioned clinical research.

Date Signature
 (Attending Doctor)

CONSENT BY VOLUNTEER FOR CLINICAL RESEARCH	R.N. Name Sex Age Unit
---	------------------------------------

Appendix B

Appendix B (i): Raw data for T_1 value measurement for phantoms using M2D FSPGR

Phantom	Measurement			Mean of measurement	Standard deviation
	1	2	3		
A	640.72	650.45	638.61	643.26	6.32
B	836.12	849.02	815.94	833.69	16.67
C	925.83	944.45	910.67	926.98	16.92
D	1440.1	1425	1459.2	1441.43	17.14
E	1761.7	1785.5	1761	1769.4	13.95
F	1326.6	1420.6	1420	1389.07	54.1
G	1655.9	1713.6	1542.6	1637.37	86.99

Appendix B (ii): Raw data for T_1 value measurement for phantoms using 3D FSPGR

Phantom	Measurement			Mean of measurement	Standard deviation
	1	2	3		
A	126.67	137.23	140.66	134.85	7.29
B	293.46	285.92	283.34	287.57	5.26
C	398.55	383.37	404.38	395.43	10.85
D	746.34	748.94	746.42	747.23	1.48
E	1107.9	1092.9	1058.6	1086.47	25.27
F	1455.7	1469.7	1484	1469.8	14.15
G	1948.8	2044	2008.5	2000.43	48.11

Appendix B (iii): Raw data for T_1 value measurement for phantoms using 3D LAVA

Phantom	Measurement			Mean of measurement	Standard deviation
	1	2	3		
A	156.84	165.59	162.45	161.63	4.43
B	265.47	257.80	264.67	262.65	4.22
C	353.61	334.07	372.40	353.36	19.17
D	667.3	579.43	557.38	601.37	58.15
E	882.19	859.16	875.22	872.19	11.81
F	1082.2	1022.8	1041.3	1048.77	30.4

G	1404.8	1476.7	1614.8	1498.77	106.72
----------	--------	--------	--------	---------	--------

Appendix C

Appendix C (i): Raw data for T_1 value of muscle measurement for volunteer using M2D FSPGR, 3D FSPGR and 3D LAVA

	Scanning technique					
	M2D FSPGR		3D FSPGR		3D LAVA	
	AXIAL	CORONAL	AXIAL	CORONAL	AXIAL	CORONAL
Volunteer 1	517.18	447.54	439.39	285.95	474.54	385.6
Volunteer 2	640.28	586.48	854.95	491.54	760.3	477.69
Volunteer 3	562.41	545.3	693.74	507.45	768.33	476.11
Volunteer 4	495.37	440.74	483.38	303.37	548.78	428.59
Mean of volunteer measurement	553.81	505.01	617.87	397.08	637.99	442.00
Standard deviation	64.05	72.33	193.14	118.65	149.02	43.96
Standard error	32.03	36.16	96.57	59.323	74.51	21.98

Appendix C (ii): Raw data for T_1 value of fat measurement for volunteer using M2D FSPGR, 3D FSPGR and 3D LAVA

	Scanning technique					
	M2D FSPGR		3D FSPGR		3D LAVA	
	AXIAL	CORONAL	AXIAL	CORONAL	AXIAL	CORONAL
Volunteer 1	165.74	147.29	50.87	50	134.67	51.31
Volunteer 2	230.07	199.82	166.21	86.23	195.64	114.38
Volunteer 3	299.83	292.19	180.57	126.95	223.19	130.42
Volunteer 4	171.82	170.21	139.01	50	165.69	85.72
Mean of volunteer measurement	216.86	202.38	134.17	78.29	179.79	95.46
Standard deviation	62.45	63.62	58.15	36.66	38.16	34.76
Standard error	31.22	31.81	29.07	18.33	19.08	17.38

